MRI-only based Radiotherapy

Line Winther Waring
&
Marie Elgaard Korsholm Nielsen

Kongens Lyngby, March 2012
IMM-MSc-2012

Technical University of Denmark
Informatics and Mathematical Modelling
Building 321, DK-2800 Kongens Lyngby, Denmark
Phone +45 45253351, Fax +45 45882673
reception@imm.dtu.dk
www.imm.dtu.dk IMM-MSc-2012

Summary

Background: Radiotherapy is used for cancer treatment and the technique requires image information of the patient's anatomy. Treatment planning is based on a CT, since the scan among other things contains information of the electron densities in the tissues. The MRI provides a high soft tissue contrast compared to the CT. Multimodality imaging is therefore increasingly used in order to give a solid base for an accurate delineation of the tumour and the neighbouring organs. However, combining the different modalities introduce a systematic registration error. The aim of this study is to evaluate if MRI-only based radiotherapy is feasible. This is investigated in order to eliminate the systematic registration error and simplify the workflow.

Materials & Methods: The investigation is performed by evaluating the dosimetric differences of a treatment plan based on an MRI as compared to a CT. The comparison is performed on four diagnostics groups; 12 head and neck patients treated with static IMRT, 6 sarcoma (extremities only) patients treated with 3D CRT, 21 prostate and 5 pelvic (not prostate) patients treated with VMAT. The data from each patient contains a CT (including a structure set), an MRI and a clinical approved treatment plan. The structure set from the CT is transferred to the MRI along with a CT-based clinical treatment plan. The transferred structure set does not include a body outline, which is therefore manually delineated in the MRI. The dose calculations based on the MRI are evaluated with a homogeneous density assigned MRI (MRI_u), and a heterogeneous density assigned MRI (MRI_b). In the MRI_u, the entire body is assigned a HU equal to water. In the MRI_b the CT segmented bone is transferred to the MRI and assigned a HU calculated based on electron densities in ICRU report 46 [38]. For HN patients, a second approach to the heterogeneous density

assigned MRI ($MRI_{b,c}$) is investigated. In addition to the MRI_b, the $MRI_{b,c}$ includes segmentation and density correction of air cavities. The differences in the dose distributions are investigated with the use of DVH points. The DVH points for the target volumes, PTV and CTV, are D_{median}, $D_{98\%}$ and $D_{2\%}$, as recommended in the ICRU Report 83 [6]. The OARs are investigated with the DVH points recommended by DAHANCA [16] and the clinical guidelines used at Herlev Hospital. For the prostate patients the differences in the dose distributions are further investigated using a gamma evaluation. The gamma evaluation is performed on the CT and the MRI_u as well as the CT and the MRI_b. The gamma evaluations are compared based on the percentage of points that fulfil the gamma criteria in the PTV.
An one-way two-tailed ANOVA and a paired t-test are used to investigate the differences in the DVH points. The assumptions of an ANOVA are fulfilled since the data is approximately normal distributed with constant variances.

Results: For the HN- , sarcoma- and pelvic patients the statistical analysis show non significant difference in the investigated DVH points. For the prostate patients the statistical analysis of the target volumes show that the MRI_u differs significant from both the CT and the MRI_b. This indicates, that a bulk density correction is necessary for the prostate patients. Similar results were found in the gamma evaluation. The analysis of the OAR for the prostate patients did not show any significant difference.

Conclusion: MRI-only based RT is found to be a feasible alternative to the CT-based RT. The results of the statistical analysis and the shape of the DVH is taken into consideration in an overall assessment of the most suitable density correction for each diagnostic group.

Resumé

Baggrund: Stråleterapi kan benyttes til kræftbehandling. En CT scanning er nødvendig forud for dosisplanlægning, idet den indeholder information om patientens anatomi og elektron densiteterne i de forskellige væv. MR bidrager, i modsætning til CT, med god kontrast i blødt væv. Ved at kombinere flere billedmodaliteter opnås en god basis for en nøjagtig optegning af tumor og det omkringliggende væv. Når de forskellige billedmodaliteter kombineres, fremkommer der en systematisk registreringsfejl. Formålet ved denne undersøgelse er, at evaluere om det er muligt at basere stråleterapi på MR. Dette er undersøgt for at eliminere den systematiske registreringsfejl og for at simplificere arbejdsgangen.

Materialer & Metoder: Undersøgelsen er foretaget ved at evaluere de dosimetriske forskelle mellem en dosisplan baseret på MR og en dosisplan baseret på CT. Sammenligningen er foretaget for fire forskellige diagnose grupper; 12 hoved-hals patienter behandlet med statisk IMRT, 6 sarkom (kun ekstremiteter) patienter behandlet med 3D CRT, 21 prostata patienter og 5 bækken (ikke prostata) patienter behandlet med VMAT. Data fra hver patient består af en CT (inklusiv et struktur sæt), en MR og en klinisk godkendt dosisplan. Struktursættet og dosisplanen fra CT er overført til MR scanningen. Struktursættet indeholder ikke information om kroppens kontur (body outline) og den er derfor optegnet manuelt på MR. Dosisberegningerne baseret på MR er evalueret med en homogen densitets-korrigeret MR (MRI_u) og en heterogen densitets-korrigeret MR (MRI_b). For MRI_u er hele kroppen tildelt en HU svarende til vand. For MRI_b er knogle optegnet på CT og overført til MR. Herefter er knogle tildelt en HU, som er beregnet baseret på elektrondensiteter fra ICRU rapport nr. 46 [38]. For hoved-hals patienter er der undersøgt yderligere en tilgang til den heterogene densitets-korrigerere MR, hvor hulrum også er segmenteret og tildelt en HU, denne benævnes $MRI_{b,c}$. Forskelle i dosisfordelingerne undersøges med

DVH punkter. De undersøgte DVH punkter for PTV og CTV er D_{median}, $D_{98\%}$ og $D_{2\%}$, disse punkter er baseret på anbefalinger fra ICRU rapport nr. 83 [6]. Risiko-organerne er undersøgt med DVH punkter anbefalet i DAHANCA [16] og retningslinjer fra Herlev Hospital. For prostata patienterne er forskelle i dosisfordelingerne undersøgt yderligere med en gamma evaluering. Gamma evalueringen er foretaget for henholdsvis CT og MRI_u og for CT og MRI_b. Gamma evalueringerne er sammenlignet baseret på den procentvise andel af punkter, som opfylder gamma kriterierne. Forskelle i DVH punkterne er undersøgt med en envejs to-siddet ANOVA og en parret t-test. Eftersom data er tilnærmelsesvis normaltfordelt med konstante varianser, er antagelserne for en ANOVA opfyldt.

Resultater: For hoved-hals, sarkom og bækken patienterne viser den statistiske analyse ingen signifikant forskel i de undersøgte DVH punkter. For prostata patienter viser den statistiske analyse for PTV og CTV af MRI_u adskiller sig signifikant fra henholdsvis CT og MRI_b. Hvilket indikerer at en bulk densitiets-korrigering er nødvendigt for prostata patienter. Lignende resultater blev fundet i gamma undersøgelsen. Analysen af risikoorganerne for prostata patienterne viser ingen signifikant forskel.

Konklusion: MRI-only baseret stråleterapi er et brugbart alternativ til CT-baseret stråleterapi. Resultaterne af den statistiske analyse og formen af DVH er taget i betragtning til en vurdering af en passende densitets-korrektion for hver diagnose gruppe.

Included in the Thesis

The thesis includes an abstract accepted for the European Society for Radiotherapy & Oncology (ESTRO) 31 Conference (See Appendix A) and a poster presented at the Department of Informatics and Mathematical Modelling (IMM), the Technical University of Denmark (see Appendix B).

A Korsholm, M.E, Waring, L.W, Paulsen, R.R and Edmund, J.M. Statistical Analysis of MRI-only based Dose Planning.*ESTRO abstract.* 2012 [28].

B Waring, L.W & Korsholm, M.E. MRI-only based Radiotherapy -An investigation of Prostate Patients. *Poster Presentation at the Department of Informatics and Mathematical Modelling.* 2011 [51].

Preface

This M.Sc. thesis is written by Marie Elgaard Korsholm Nielsen & Line Winther Waring. The thesis was produced between the 5th of September 2011 and the 5th of March 2012 (corresponding to 30 ECTS points) at Copenhagen University Hospital, Herlev, the Department of Oncology (R). The work has been done in co-operation with the Department of Informatics and Mathematical Modelling at the Technical University of Denmark.
The thesis is performed in fulfilment of the requirements for acquiring an M.Sc. in Medicine & Technology at the Technical University of Denmark (DTU) and the University of Copenhagen (KU).

Supervisors:

Jens M. Edmund, PhD, DABR
Copenhagen University Hospital, Herlev
Department of Oncology (R)

Rasmus R. Paulsen, Associate professor
Technical University of Denmark
Department for Mathematical Modelling (IMM)
Section for Image Analysis and Computer Graphics

Danmarks Tekniske Universitet, Lyngby, 05-March-2012

Line Winther Waring

Marie Elgaard Korsholm Nielsen

Acknowledgements

We wish to thank the staff at the Department of Oncology (R), Herlev Hospital for making us feel welcome throughout the project. Moreover we wish to thank the staff and co-students at the Department of Informatics and Mathematical Modelling for their continuous counselling and inspiration at the weekly meetings and workshops. We would like to thank Karl Sjöstrand (IMM) for his statistical guidance and Claus Behrens (Herlev Hospital) for his helpfulness.

Additionally, we would like to thank family and friends for their support and interest throughout the project, especially Rikke Eiland for her great company and constructive feedback of our ideas and project drafts.

A great thanks to Rasmus R. Paulsen for his guidance, support, patience and always positive approach to our project.

Finally, a special thanks to Jens M. Edmund, for his enthusiasm, engagement and great help with the project. Without his help and continuous guidance this work could not have been accomplished.

Contents

Acronyms & Glossary

3DCRT	3-Dimensional conformal radiotherapy. A technique where the target is irradiated using static angles and static apertures [27, p. 413].
ANOVA	Analysis Of Variance [24, 406].
BEV	Beams eye view. A display of a plane perpendicular to the central axis of the beam viewed from the point of origin [27, p. 207].
CBCT	Cone Beam Computed Tomography. A 3D data set generated from planar projection images [27, p. 216].
CERR	Computational enviroment for radiotherapy research [1].
CT	Computed Tomography. Medical imaging method used to generate a 3D image from 2D X-ray images [11, p. 6].
CTV	Clinical Target Volume. A volume that contains the GTV and tissue believed to have subclinical malignant tissue relevant for radiotherapy [6].
DAHANCA	Danish Head & Neck Cancer Group [16].

DRR	Digital Reconstructed Radiographs. Digitally simulation of the passage of X-ray through the patient's CT representation [6].
DTA	Distance to agreement [31].
DVH	Dose Volume Histogram. The DVH illustrates a 3D dose distributions in a graphical 2D format [6].
Dxt.	Dexter.
FID	Free-induction-decay.
FID	Repetition time.
GAH	Gamma Histogram. A cumulative histogram describing a 2D γ -map [47].
GTV	Gross Tumour Volume. The primary tumour (the visible cancer tissue) [6].
GVH	Gamma Histogram. A cumulative histogram describing det gamma index relative to an investigated volume [47].
Gy	Gray. J/kg.
HN	Head and Neck.
HU	Hounsfield Unit [21, p. 2].
ICRU	International Commission on Radiation Units and Measurements [6].
IMRT	Intensity-Modulated Radiotherapy. A technique where the radiation is given with static angles and a dynamic aperture [27, p. 413].
ITV	Internal target volume. The CTV plus a margin that accounts for internal motion [6].
LINAC	Linear Accelerator.
MLC	Multileaf collimator. The MLC consist of tungsten leaves, used to create complex beam shapes and vary beam intensity [9].

MRI	Magnetic Resonance Imaging Medical imaging method that make use of the properties of the nuclear spin to create images with an external magnetic field [11, p. 9].
$MRI_{b,c}$	Bulk density assigned MRI including density correction of air cavities.
MRI_b	Bulk density assigned MRI.
MRI_u	Unit density assigned MRI.
MU	Monitor units. Measure of machine output of radiation for radiotherapy.
NS	Non-significant.
OAR	Organs at risk. Volumes of normal tissues that could be affected in the treatment of radiation [6].
PD	Proton density.
PET	Photon Emission Tomography. Tomographic images reconstructed from positron. Provides a diagnostic functional information [11, p. 9].
PRV	Planning organ at risk volume. A margin added to the OAR [6].
PTV	Planning Target Volume. The PTV is the clinical target volume and a margin that account for uncertainties such as variation in the patient setup into consideration [6].
QA	Quality-assurance.
QQ-plot	Qantile-quantile plot [35, p. 64].
QUANTEC	Quantitative Analysis of Normal Tissue Effects in the Clinic [32].
RA	RapidArc. Radiotherapy technology from Varian Medical Technology that uses the theory of VMAT. The delivery of radiation is a 360 degree rotation of linearly accelerators [2].

RF	Radio frequency [11, p. 415].
RT	Radiotherapy. Treatment with ionizing radiation.
S	Significant.
SSD	Source-to-skin distance [27, p. 35].
Sin.	Sinister.
TE	Echo time.
TPS	Treatment Planning System. Software used to generate and evaluate treatment plans [15].
UTE	Ultra-short echo time. A sequence designed to visualize tissues with a short T2 [26].
VMAT	Volumetric Modulated Arc Therapy. A technique where the radiation delivered from dynamic angles with a dynamic aperture [40].
VOI	Volume of interest [27, p. 35].

List of Figures

List of Tables

Chapter 1

Introduction

Cancer treatment with radiotherapy (RT) requires image information of the patient's anatomy. A full virtual 3D representation of the patient can be obtained with the use of imaging techniques, such as X-ray computed tomography (CT) and magnetic resonance imaging (MRI). The CT and the MRI visualize different tissue properties and are often combined to obtain all complementary anatomical information. The combination gives a solid base for a more accurate delineation of the tumour and the neighbouring organs. These image modalities can be combined with functional imaging techniques, such as positron emission tomography (PET) [43, p. 179].

Multimodality imaging is increasingly combined for a better tumour delineation. The CT is used because of a high geometrical accuracy and the direct connection to electron density [25]. The MRI provides additional soft-tissue contrast to the CT and the scans are therefore co-registered. However, the registration of MRI and CT introduce a systematic registration error. Further, adaptive radiotherapy introduces an increase in the number of scans and the potential for additional systematic registration errors. A possible alternative to the CT-based radiotherapy is MRI-based radiotherapy where the CT is replaced with an MRI in all steps of the treatment workflow.

The replacement of the CT can potentially lead to a simplified workflow and a decrease in the time consumption, costs, and radiation exposure to the patient

[25]. The radiation exposure is however less significant in RT, as the patient is already treated with radiation. Some challenges must be overcome in order to eliminate the CT. These challenges concern dose calculations and positioning of the patient without the CT information.

In this study four diagnostic groups are investigated; 12 Head and Neck (HN) patients, 6 sarcoma (extremities only) patients, 21 prostate patients and 5 pelvic (not prostate) patients.
The aim of this study is to compare dose distributions based on an MRI and a CT, respectively.

Chapter 2

Previous Related Work

Previous studies have investigated MRI-only based radiotherapy. Two related studies will be described in the following, a study performed by Jonsson et al.[25] and Lambert et al.[29].

Jonsson et al. describes the MRI as a complement to CT in radiotherapy. This was done by comparing the dose distributions based on a CT as well as an MRI for different treatment regions. Each dose calculation was performed with the same field setup, using tree-dimensional conformal radiotherapy (3D CRT). The study was performed on four diagnotic groups; head & neck -, prostate-, thorax- and brain cancer. Each group contained 10 randomly selected patients.

The dose calculation was compared for: 1) A clinical CT 2) A CT where all tissues inside the body outline is assigned a density equal to water 3) A bulk density assigned CT 4) A bulk density assigned MRI.
The bulk density correction is performed by giving similar tissues the same mass density. Therefore all bone tissues are assigned the same mass density. Additionally, is a mass density assigned to the soft tissue and air cavities, respectively. The chosen mass densities are based on recommendations from ICRU Report 46 [25]. It should be noted that no MRI information was available for the head & neck patients. The comparison was therefore based on the clinical CT and the density corrected CT.

Jonsson et al. illustrate with their study that the use of MRI-only in dose calculations is feasible. However, they find that a broader analysis is needed prior to a clinical implementation. Our study contributes with further research, including the use of MRI combined with different treatment techniques and the effect of different density corrections.

Lambert et al. investigate the accuracy of a dose calculation based on a bulk density assigned MRI as compared to a CT for radiotherapy of the prostate patients.

The patient dataset contains 39 prostate patients between 54 and 79 years, with a CT and a whole-pelvic MRI. The patients were treated with 3D CRT [29].

In order to compare the CT and the MRI; a CT (gold-standard plan), an uniform- and a bulk density CT were created. Additionally, two MRIs were created; an uniform- and a bulk density corrected MRI. Lambert et al. determines the bone density based on effective depth calculations. The CT-based RT plan was transferred to the MRI and the same plan was therefore used to calculate the dose distributions based on the CT and the MRI. The comparison of the dose distributions is based on a statistical analysis.

Lambert et al. found that MRI-based RT is feasible when using a bulk density corrected MRI [29].

The results of the two studies described above will be discussed with relation to our study in Section 11.7.

Chapter 3

Radiotherapy Planning Process

The following chapter explains each step in the RT planning process. The steps are summarized in Figure 3.1.

Patient Treatment Positioning and Immobilization

In radiotherapy it is important that the patient is positioned in the exact same way during the image acquisition and the subsequent RT [17, p. 39-40]. The treatment delivery is divided into fractions where the patient receives a small amount of radiation in a given period until the total prescribed dose is reached. This is done in order to optimize the therapeutic ratio. The therapeutic ratio is the ratio of maximal tumour control and minimal damage to the healthy tissue [7]. Since RT is divided into several fractions, it is very important that the treatment delivery is reproducible.

The proposed treatment position of the patient is determined in the initial part of the planning process. Moreover, an immobilization device is fabricated to reproduce the patient position. Fixation equipment such as a support for the hips and the legs are shown in Figure 3.2(a) and a thermoplastic mask to fixate

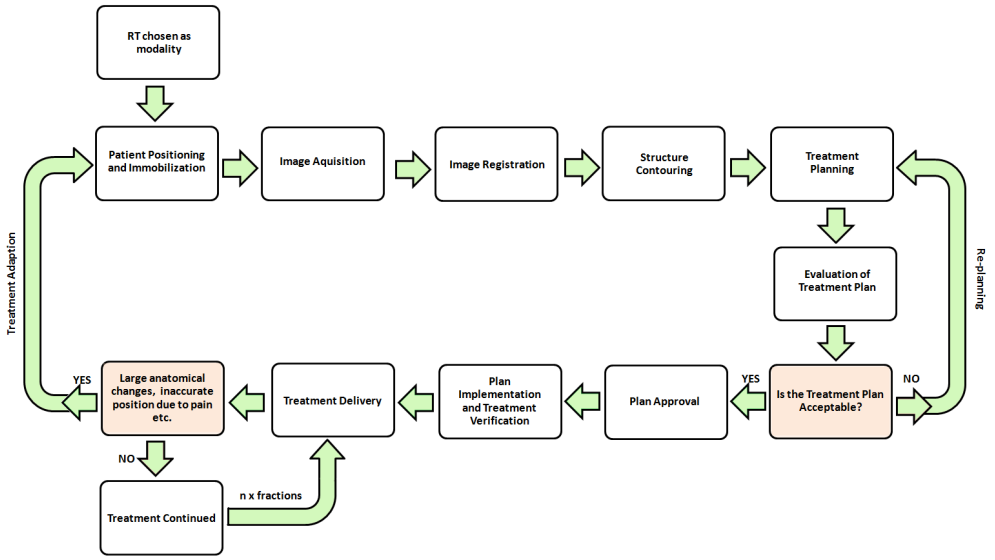

Figure 3.1: The process of RT. The first step in the cycle is choosing RT as modality.

the head is shown in Figure 3.2(b). Inadequately patient immobilization may result in deviation from the initial setup during treatment that should lead to a new planning cycle (see Figure 3.1).

Markers are placed on the patients skin and the immobilization device to serve as fiducial marks for traceability and verification of the treatment setup [43].

(a) Fixation of legs (b) Fixation of head

Figure 3.2: The immobilization equipment is used to fixate the patient during the RT, in order to deviations in the patient setup [46].

Image Acquisition

A CT is performed where the patient is placed in the treatment position. The CT is the primary source of image data for radiotherapy. However, there is an increasing demand for other image modalities such as MRI. The concepts of CT and MRI will be described in Chapter 4.

The tumour-soft tissue contrast in an MRI provides additional information for a tumour delineation, as compared to CT. PET is an imaging modality that is used to provide functional information and is increasingly used for imaging of e.g. lung cancer [43].

When using other imaging modalities in addition to a CT the patient positioning during the image acquisition must be in accordance with the intended treatment setup. This must be done in order to perform a registration of the images.

Image Registration

When using multiple image modalities, the CT is co-registered with the additional image study. Image registration is the process of overlaying two images of the same scene [53]. The image registration is a geometrical alignment of the two images, where one of the images are considered as the reference image, in RT the CT is the reference image. An additional image modality e.g. the MRI is considered as the source image. The image registration is a critical step in the RT planning, since the registration is required to obtain complete information of the anatomy of the patient to make the most accurate structure contouring [43]. The image registration will introduce an error, which is caused by the use of different sources (multimodality imaging) and the time difference between the scans [53]. Errors due to time difference can be small anatomical changes that might occur, if the scans are not being performed subsequently. Additionally, imperfect patient repositioning will occur when the patient has to shift from one scanner to the next.

The registration error will influence all of the following steps of the RT process (see Figure 3.1). A systematic registration error will therefore be present in all treatment fractions. A motivation for MRI-only based RT is to eliminate the systematic registration with the use of a single image modality.

Delineation of Target Volumes and Organs at Risk

Delineation of the target volumes and the OAR based on the image data is typically performed by the oncologist. The image data is displayed and the contours are drawn manually slice-by-slice as seen in Figure 3.3. Some organs have well-defined boundaries and can be contoured semi-automatically, which is e.g. the case for the lungs. Other OARs require a fully manual delineation [43]. The manual delineation is a very time consuming step in the RT planning.

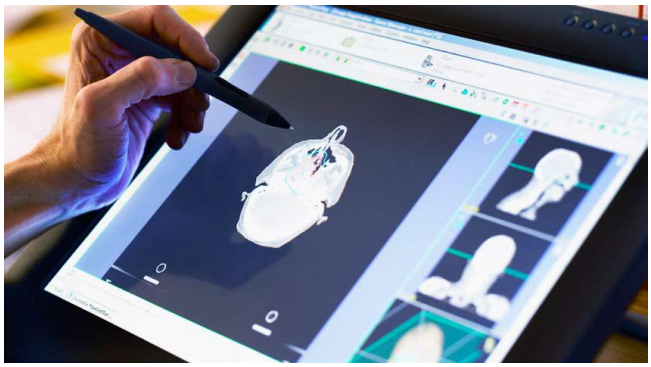

Figure 3.3: An oncologist delineates the tumour and the OARs manually slice-by-slice on the image data [46].

The delineated structures are referred to as the structure set. The images and the structure set are handed over to the medical physicist or dosimetrist that is responsible for the treatment planning.

Treatment Planning

The next step in the treatment planning process, is the design of a treatment plan. This includes a beam arrangement and design of the field apertures. The delivery technique is based on the specific diagnostic group and the tumour localisation along with the clinical established protocol and practice. The treatment planning system (TPS) can simulate the treatment delivery (treatment technique and dose distribution) of the linear accelerator. A 3D model view is displayed in Figure 3.4. In the plan, it has to be taken into consideration that the dose to the healthy tissue does not exceed the tissue specific tolerance limit. Moreover, the tumour coverage must not be compromised. RT planning can be performed as forward or inverse planning, dependent on the delivery technique.

Typically, in forward planning the beam arrangement is selected based on clinical experience. After the beam geometry is designed, the dose distribution is calculated. The beam arrangement can be modified based on an evaluation of for e.g. isodoselines or the dose distribution shown in a colour wash. In an inverse planning, the dose distribution criteria are predefined and the treatment plan is optimized to meet these criteria [27, p. 430]. An inspection of the calculated 3D dose distributions in the transaxial plane forms the basis of a clinical evaluation together with a dose volume histogram (DVH). In the DVH the 3D dose distribution is reduced to an easily understandable 2D format [43]. The DVH will be described later in Section 7.1.

The treatment plan must be approved by the oncologist and the medical physicist before the patient starts the treatment [43].

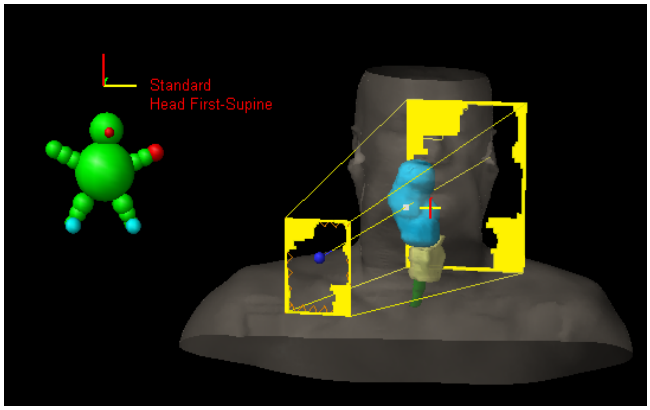

Figure 3.4: A 3D model view, showing the beam of 340 degree (Cancertype: Head & Neck, Patient ID: HN18).

Plan Implementation and Setup Verification

To confirm the patient positioning, digitally reconstructed radiographs (DRR) generated by the TPS from the CT scan are compared to the radiographs acquired with the linear accelerator (LINAC) [37, 43]. If the deviation between the DRR and the radiographs is acceptable will the treatment proceed. If the deviation is not acceptable the patient will be repositioned.

To confirm the validity and accuracy of the designed, evaluated, and approved treatment plan, patient specific quality-assurance (QA) is performed. This includes isocentre placement check on the LINAC, beam parameter settings etc.

The isocentre placement check is performed with a laser system, where the laser is adjusted after the previous mentioned marking system. In addition to the patient specific QA, machine QA is performed. The machine QA includes e.g. control of the accelerator performance.

Treatment Delivery

Different delivery techniques are used depending on the diagnostic group. This study includes three treatment delivery techniques (3D CRT, intensity modulated RT and volumetric modulated arc therapy), these will be described in Chapter 6. Figure 3.5 displays the patient positioning in the LINAC simulated by the TPS.

The patient will often receive a standard fractionation of 2 Gy daily with a total treatment dose of 50-70 Gy [12, p. 30]. The treatment period differs dependent on the diagnosis and the cancer stage. During the treatment period the treatment will be evaluated. Prior to each treatment, the patient positioning is validated. Sometimes the tumour's response to the treatment is verified and an adaptive dose plan is considered (See Figure 3.1).

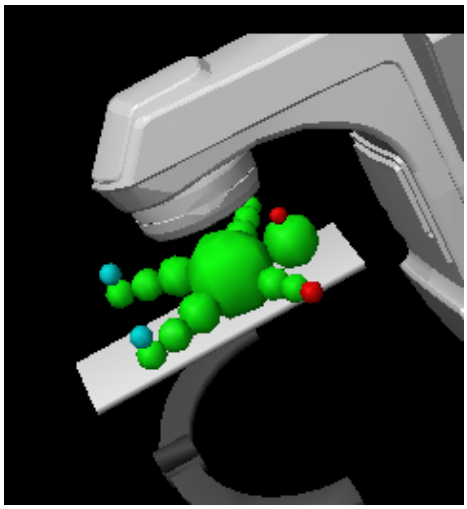

Figure 3.5: The patient positioning in the treatment machine simulated by the TPS.

Chapter 4

Image Acquisition

4.1 X-ray Computed Tomography

In X-ray computed tomography (CT), transaxial X-ray projections are computed to create images of the body. The X-ray tube rotates around the body, while the beams pass through the patient at different angles. The intensity of the attenuated beams is measured with detectors placed opposite the X-ray tube. The intensities are converted into electric signals in the detectors. To compensate for inhomogeneities in the system, the signals are amplified and processed. The processed signals are transformed into attenuation values which is the CT raw data [19, p. 8-9]. The raw data is reconstructed into an image, most often using the filtered back projection algorithm [21, p. 6]. In the filtered back projection algorithm, the attenuation values are assigned to each pixel in the image matrix. Adding the values from each projection reinforces the areas of high as well as low attenuation [11, p. 330-331]. The reconstructed CT image is a grey tone image, where each pixel represents a scanned voxel with a Hounsfield unit (HU). The HU describes the degree of attenuation relative to water [11, p. 356]:

$$\mathrm{HU}(i,j) = 1000 \cdot \frac{\mu_{(i,j)} - \mu_{\mathrm{water}}}{\mu_{\mathrm{water}}} \tag{4.1}$$

where $\mu_{(i,j)}$ represents the linear attenuation coefficient of the voxel ij, and

μ_{water} is the linear attenuation coefficient for water at the same spectrum of photon energies. The HU is therefore dimensionless.
The HU describes the absorption properties of the tissue in the different voxels. However, a HU cannot give an exact definition of the tissue type the voxel belongs to, since the tissue types often consist of more than one component [21, p. 3].

By definition, a HU that equals to zero will correspond to water (See Equation 4.1). An overview of HUs for different human tissues are shown in Figure 4.1. The contrast in the CT image is caused by different HUs. Bone and contrast agents appear bright in the image, air is black and soft tissues are different shades of grey. The similarity in the HU for different types of soft tissue makes it difficult to differentiate between theese tissue types. The HU that corresponds to tumour tissue is in the same range as soft tissue (See Figure 4.1), which makes it difficult to differentiate between tumour tissue and healthy tissue.

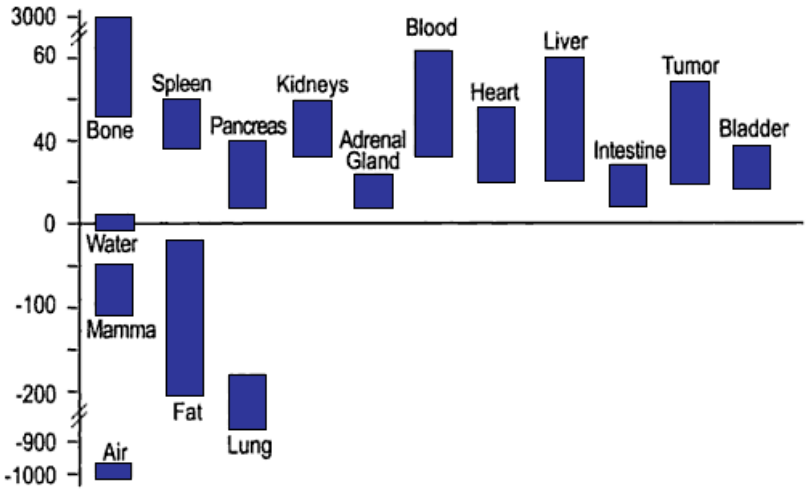

Figure 4.1: An overview of HUs for human tissues [39, p. 416].

Figure 4.2 illustrates a CT image of the brain. It is seen that bone and air cavities are very well defined, but the soft tissues is hard to differentiate.

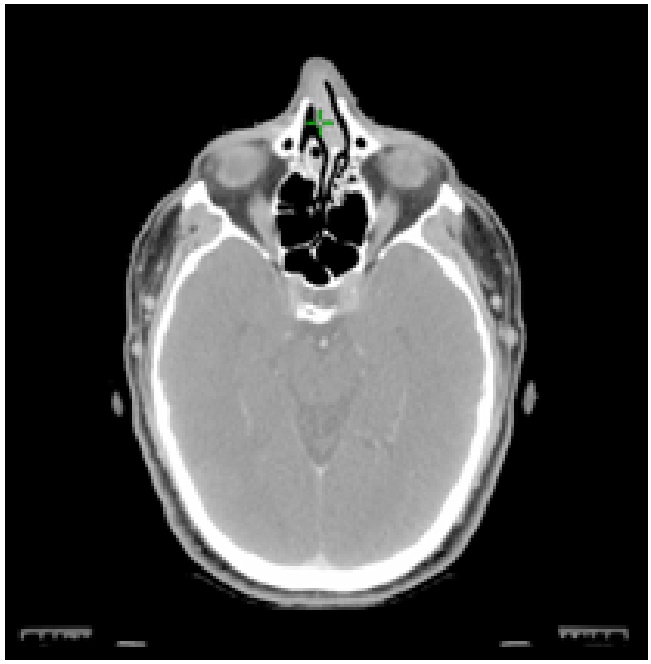

Figure 4.2: A transaxial CT image of the brain (Cancertype: Head & Neck, Patient ID: HN10).

Calibration curve

As mentioned above, the HUs describe the degree of attenuation of the X-rays relative to the attenuation of water. For photon energies between 0.5 - 5 MeV, the attenuation of the X-rays is primary caused by Compton scattering. The Compton scatter is the result of interactions between photons and electrons. When the photon interacts with the electron, energy is transferred to the electron and the scattered photon will retain the remaining energy [22, p. 15]. The density of the tissue is one of the physical properties that influence Compton scatter, and thereby creates the contrasts in the CT images [11, p. 356].
In the TPS (Eclipse, Varian Medical Systems) the HUs are converted into electron densities based on a CT calibration curve. The default calibration curve is given as:

$$\rho^{\omega,e} = 1.0 + 0.001 \cdot \mathrm{N_{CT}},\ -1000 \leq \mathrm{N_{CT}} \leq 100 \tag{4.2}$$

$$\rho^{\omega,e} = 1.052 + 0.00048 \cdot \mathrm{N_{CT}},\ \mathrm{N_{CT}} \geq 100 \tag{4.3}$$

where $\rho^{\omega,e}$ is the electron density relative to the electron density of water and $\mathrm{N_{CT}}$ is the CT number (HU).

The CT calibration curve is sketched in Figure 4.3

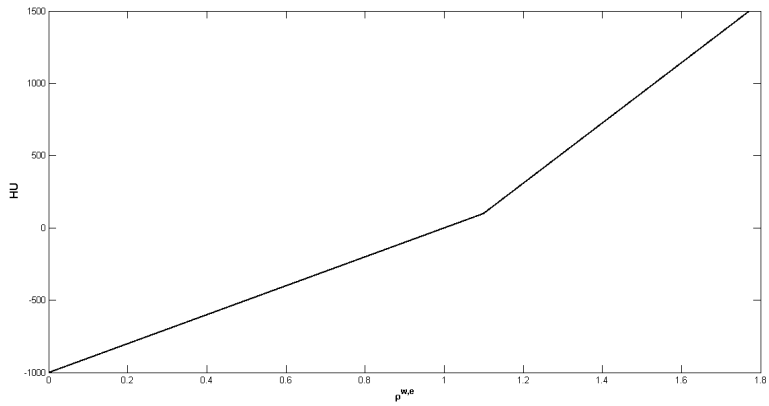

Figure 4.3: The CT calibration curve

4.2 Magnetic Resonance Imaging

Magnetic resonance imaging (MRI) makes use of the fact that approximately 75 % of the human body consists of water and takes advantage of the physical properties of hydrogen [34, p. 31]. The MRI technology therefore gives excellent images of soft tissues, which are water-based tissues.

MR images are produced by MR pulse sequencing. The required image is obtained with a sequence that consists of radio frequency (RF) pulses and MR gradients which is applied with controlled duration and timings. By modifying the repetition time (TR) and the echo time (TE) the required image contrast and signal intensity is obtained for the diagnostic purpose. The TR is the time between the initial RF pulses in each repetition in the sequence. The TE is the time from the initial RF pulse until a signal is measured (the echo) [34, p. 13,31-33].

The most important properties of the MRI technology are the relaxation times, denoted T1 and T2, which are related to the spin of the nuclei (^{1}H). The relaxation times describe the time it takes for the nuclei to return to equilibrium after being flipped by a RF pulse. During the relaxation, a free-induction-decay (FID) is produced, which can be measured in a coil.
The relaxation time of protons in different tissues is used to create contrast in the image by changes in the TE and the TR [34, p. 13,31-33]. A third relaxation time, T2*, is a combination of T2 and the inhomogeneity of the external magnetic field [34, p. 31-38].

In Figure 4.4, two MR images of the same patient are shown with different weightings. Figure 4.4(a) shows a T1 weighted MR image. T1 is the relaxation time for the longitudinal magnetisation recovery. To obtain the T1 weighted image, a short TR and a short TE are used. In a T1 weighted image, the fat-based tissues will appear brighter than water-based tissues, which are mid-gray. Fluids usually appear dark. T1 weighted images are often used for anatomical purposes, due to excellent contrast [34, p. 32].

Figure 4.4(b) shows a T2 weighted MR image. T2 is the relaxation time for the transverse magnetisation recovery. A T2 weighted image requires a long TR and a long TE. In a T2 weighted image, water will have a higher signal than fatty tissues, therefore fluids will appear bright and tissues appear mid-grey. Since a collection of fluid will appear bright, the T2 weighted MR image is often used for pathological purposes [34, p. 33].

As described in Section 4.1 the contrast in the CT images are caused by different attenuation properties in the tissues. A similar relation between contrast

densities in the tissue is not seen in the MR images. In the MRI the contrast in the images are created based on a linear look-up table, where the magnitudes of the measured signals are converted to a grey tone in the range of [0 255] [18, ch. 10].

Proton density (PD) is related to the number of hydrogen atoms in a volume. Fluid, such as cerebrospinal fluid, has a high PD, in contrast to bone that has a low PD. Magnetic susceptibility is defined as the extend to which a tissue becomes temporarily magnetized when it is placed in a magnetic field, which depends on the arrangement of the electrons in the tissue. Bone and air appear dark in the MR image, due to low PD and low susceptibility [34, p. 31, 39, 102]. Moreover, bone has a very short T2 relaxation time, which makes it difficult to image the bone structures.

In contrast to the MRI, the CT has a good capability to image the bone but a poor capability to image soft-tissue [23]. MRI provides excellent facilities to investigate soft tissue and is therefore a great tool for diagnostic purposes. However, MRI has as previously mentioned a poor definition of bone, due to a small number of hydrogen nuclei, a low susceptibility and a short T2 [26]. As MRI has increasingly become the primary diagnostic tool, it would be ideal if MRI could be used to image bone and soft tissue in the same scan session. Recently, an ultra-short echo time (UTE) sequence has been investigated to image bone. UTE makes use of a very short TE time in order to capture the signal from bone before it decays (the signal decays fast due to a short T2 relaxation) [26]. The ability to image bone with MRI opens up for new MRI applications [23].

In our study, MRI-only based radiotherapy is investigated with the assumption that a pulse sequence such as UTE gives the ability to image the bone structure with MRI.

(a) A T1 weighted MR image of the brain

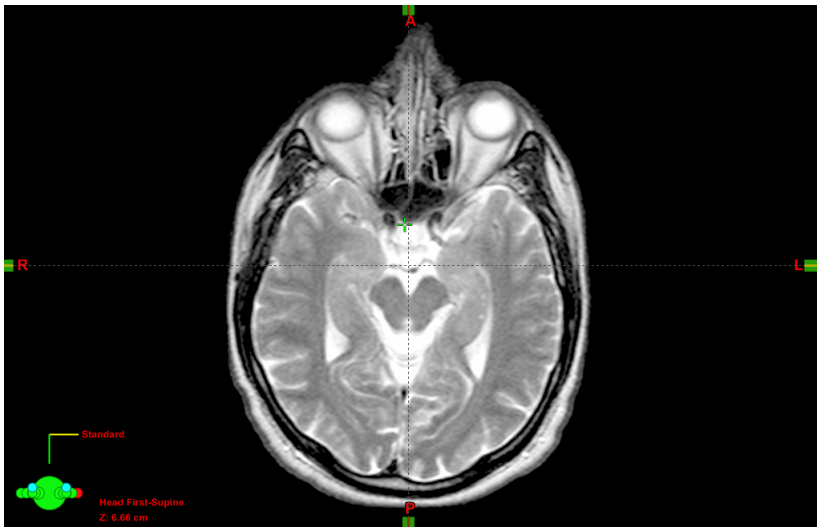

(b) A T2 weighted MR image of the brain

Figure 4.4: The MR images appear different dependent on the weighting of the image. (Cancertype: Head & Neck, Patient ID: HN10).

Chapter 5

Definition of Volumes

The structure set contains the target volumes and the OAR, which are delineated to be used in the treatment planning and reporting processes in RT [6].

The following structures are often included in the structure set:

- GTV: Gross tumour volume
- CTV: Clinical target volume
- ITV: Internal target volume
- PTV: Planning target volume
- OAR: Organ(s) at risk
- PRV: Planning organ at risk volume

The volumes are displayed as a graphical representation in Figure 5.1.

The GTV, CTV and OAR are volumes delineated based on an anatomical knowledge. The PTV, PRV and ITV are non-anatomically volumes which are created to account for internal organ motion and external patient movement.

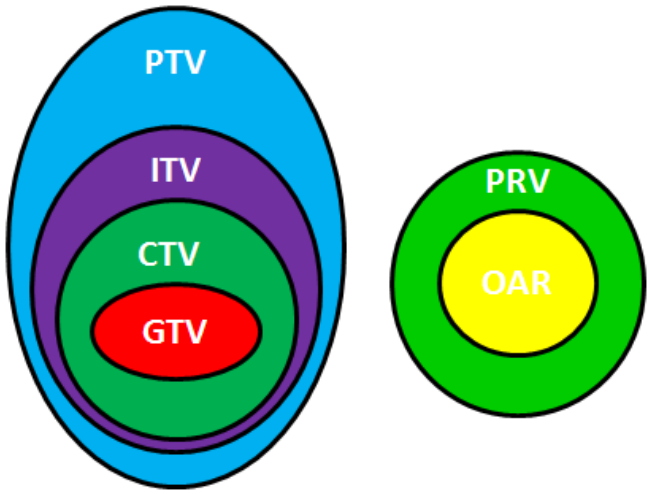

Figure 5.1: A graphical presentation of the volumes. Inspired by [44].

The GTV consists of the primary tumour. The GTV is macroscopic and is therefore defined as the visible cancer tissue. Usually, the GTV is based on a clinical evaluation. If the GTV is delineated on the MRI and transferred to the CT, a systematic registration error will be introduced.

The CTV is the volume that contains the GTV and the surrounding tissue that is expected to contain subclinical malignant tissue relevant for RT. Subclinical malignant tissue includes microscopic tumour spread from the primary tumour and can by definition not be visualized in a scan.

The ITV is defined as the CTV with a margin that makes up for shape and position (internal movement) of the CTV. The ITV ensures that all of the tumour is irradiated, taking organ motion into consideration. This means that the ITV will be larger when treating a lung tumour compared to the ITV when treating a brain tumour, since respiration will contribute to internal motion.

The PTV is used for the treatment planning and evaluation to ensure that all parts of the CTV will receive the prescribed dose. The margin of the PTV takes uncertainties due to variation in the patient setup into consideration. The delineation of the PTV usually includes the ITV, and the volume therefore considers both the internal and external variation.

The OARs are healthy tissue that are proximate to the PTV and will receive a significant amount of radiation during the RT. If the OAR are irradiated, the consequence could be dysfunction. The OAR can be divided into serial and

parallel organs. The serial organs consist of a chain of functional units, where each unit has to be preserved in order to maintain full functionality. The parallel organs are independent functional units [6].

The PRV takes variation in the position and anatomical changes of the OAR into consideration, similar to the PTV.

In Figure 5.2 the target volumes; GTV, CTV and PTV are delineated for a HN cancer patient. Two OARs and a PRV are also visualised, the medulla (including medulla PRV) and the parotid glands. The medulla is an example of a serial organ, since destruction of a nerve will effect the functionality of the nerves downstream. The parotid glands are parallel organs, as dysfunction of some subunits will not effect the overall functionality of the organ.

For some patients, more than one target volume is defined in the structure set. This can for example be the lymph nodes that are suspected to contain cancer cells. These lymph nodes have an individual prescribed dose and therefore requires another PTV.

In this study, the focus is the primary target volumes. In most cases this is the PTV-Tumour and the CTV-Tumour, which are the target volumes that cover the tumour volume. Exceptions can occur where the PTV and CTV are cropped to fit the body outline (DVH-PTV and DVH-CTV). In these cases the cropped target volumes are investigated. The target volumes are only referred to as the PTV and the CTV in this study.

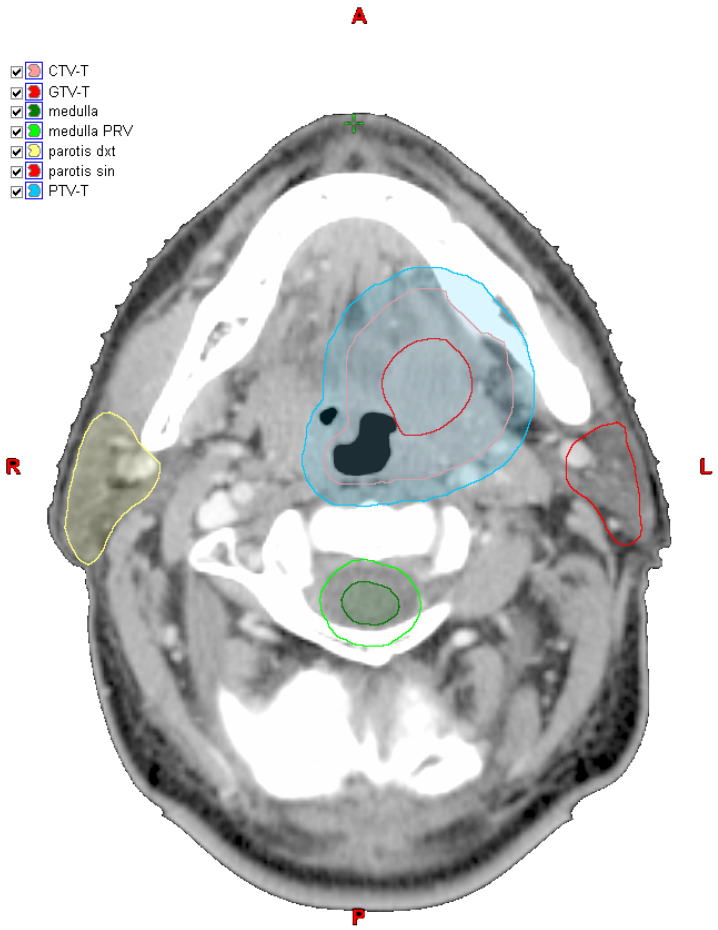

Figure 5.2: The GTV, CTV, PTV, medulla, medulla PRV and parotis sin./dxt. delineated in a CT image of a HN patient (Cancertype: Head & Neck, Patient ID: HN23).

Chapter 6

Treatment Delivery

6.1 The Linear Accelerator

In radiation therapy, a linear accelerator (LINAC) is used to generate radiation that is aimed precisely towards the patient. The radiation interacts with the cells and destroys the DNA [14, p. 339]. A schematic representation of the LINAC is seen in Figure 6.1

The electron gun is the source of the electrons. The electron gun controls the dose rate rapidly and accurate. The electrons from the electron gun are lead into the waveguide. The waveguide accelerates the electrons into nearly the speed of light with the use of micro waves (RF waves). The RF waves are emitted into the waiveguide from the RF power generator in synchrony with the electrons from the electron gun [33, 37].

The electrons enter a 270 degree bending magnet that ensures that the electrons do not loose their energy while the direction of the beam is changes towards the patient. Additionally, it acts as an energy spectrometer. The beam of electrons leave the bending magnet and hit a target, usually of tungsten, causing it to emit bremsstrahlung [33].

The multileaf collimators (MLCs) shape the beam to fit the PTV, to ensure

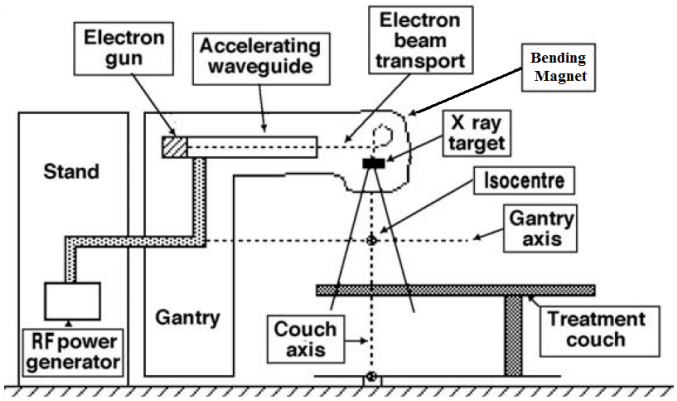

Figure 6.1: A schematic presentation of the LINAC. Modified from [42, p. 140].

that the PTV is irradiated while sparring the healthy tissue [33]. The MLC consist of tungsten leaves. The leaves acts as a shield and therefore collimates the beam [9], see Figure 6.2.

The beam of radiation is delivered from the gantry head. By rotating the gantry, the radiation can be delivered from different angles. Three-dimensional conformal radiation therapy (3D CRT), intensity modulated radiation therapy (IMRT) and volumetric modulated arc therapy (VMAT) are delivery techniques that are used to optimize the therapeutic ratio. These techniques will be explained in the following.

6.1.1 Three Dimensional Conformal Radiotherapy

In three dimensional conformal RT the target volume is irradiated from different static angles and with static apertures. To ensure maximum dose to the target volumes and minimum dose to healthy tissue, the beam is conformed as closely as possible to the target volume at each angle [27, p. 413-414]. 3D CRT is planned with forward planning where the beam is shaped with the MLCs in order to fit the target volume from the beams eye view (BEV)[20]. An example is seen in Figure 6.3, where the treatment plan for a sarcoma patient is shown in the BEV from one beam angle. It is seen that the beam is conformed with the MLC to fit the PTV. All the sarcoma patients in our study are treated with 3D CRT.

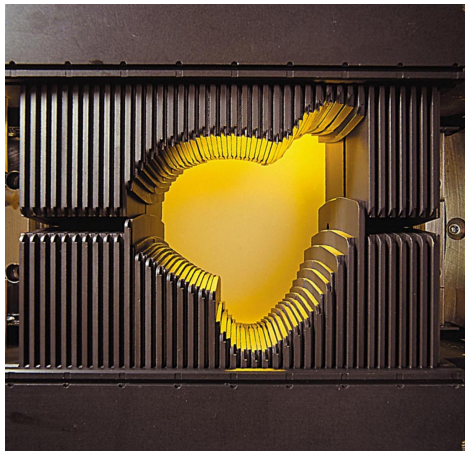

Figure 6.2: A MLC, the leaves are positioned in order to create a specific field aperture [3].

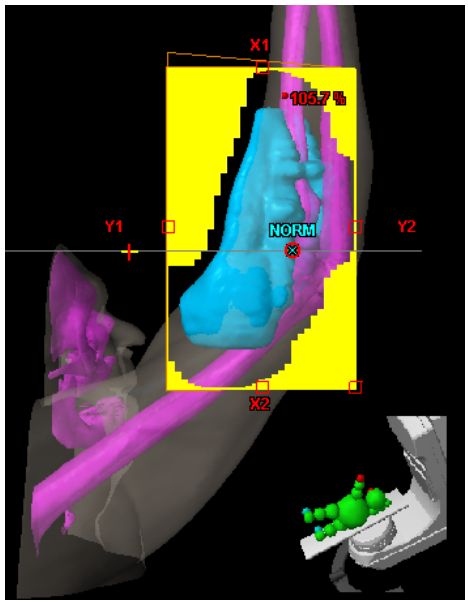

Figure 6.3: A sarcoma patient treated with 3D CRT, seen from the BEV (180 degrees). The purple area is the bone. The blue area is the PTV. (Cancertype: Sarcoma, Patient ID: Sar7).

6.1.2 Intensity Modulated Radiotherapy

In intensity modulated radiotherapy (IMRT), the radiation is given from static angles with a dynamic aperture. IMRT is a technique where the intensity of the beam is adjusted in order to deliver a non-uniform intensity to the target volume in each beam direction. The intensity modulated beam from different directions makes it possible to achieve the desired dose distribution in the irradiated volume. The varying intensity introduces an additional degree of freedom, compared to 3D CRT [9].

The principle of the intensity modulated beams is seen in Figure 6.4. In this example the target is the prostate, and the rectum is the OAR. It is seen that the beams are modulated so that the largest amount of radiation are given in the areas where the rectum is the least affected. At the same time the different angles will ensure that the whole target volume is covered.

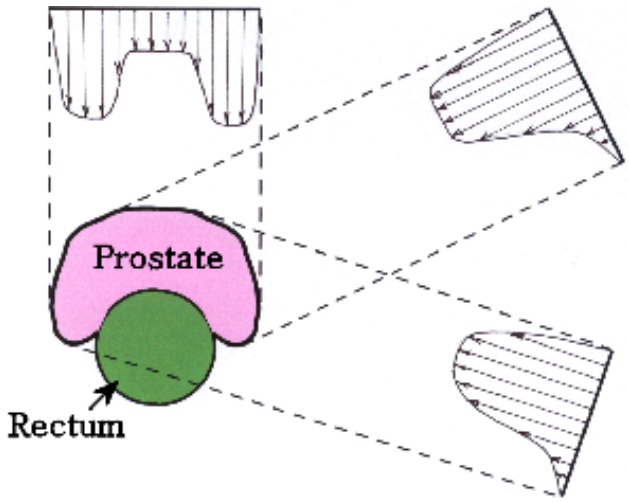

Figure 6.4: The prostate and the rectum irradiated from 3 directions, where the intensity of the beams are modulated in order to radiate the prostate without compromising the rectum [4].

The technique is based on inverse planning algorithms. The optimization process involves determining which intensities that corresponds to the predefined dose distribution criteria [27, p. 430].

The intensity of the beams are modulated using dynamic MLC created apertures. The treatment can be performed as a dynamic method where the MLC

leaves move from one side to the other of the aperture with different velocities while the beam is turned on. This is known as the "sweeping gap" technique [27, p. 432-433].

6.1.3 Volumetric Modulated Arc Therapy

In volumetric modulated arc therapy (VMAT) the radiation is delivered from dynamic angles with a dynamic aperture. In VMAT, the radiation is delivered with a continuously varying beam. The gantry rotates in one or several arcs around the patient with varying dose rate, MLC opening and gantry speed. VMAT differs from other techniques where the gantry is static, when the radiation is delivered, which increases the degrees of freedom [52].

A treatment plan contains a sequence of control points, these are seen as the red bars in the circle in Figure 6.5. At each control point, the MLC position and gantry angle should correspond to a given number of cumulative monitor units (MU). In order to fulfil these specifications the dose rate, MLC and/or gantry speed can be adjusted. The control points act as quality assurance to ensure that the planned dose is delivered correct [50].

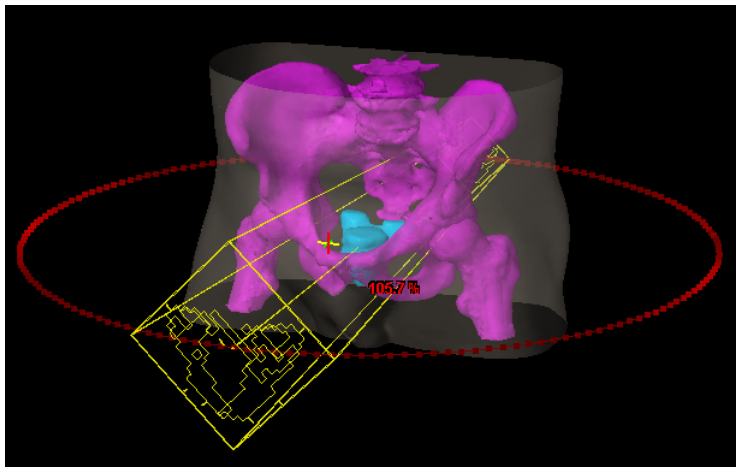

(a) The PTV(blue area) and the bone structure (purple area).

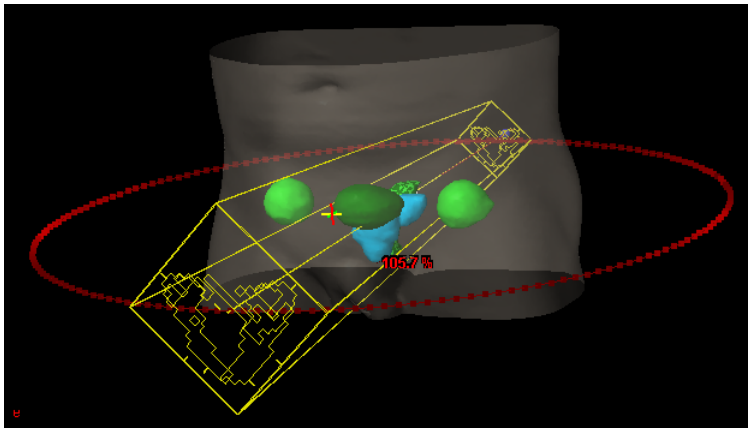

(b) The PTV and OARs for a prostate patient. The OAR: Caput femoris (light green area), bladder (dark green area) and rectum (two-coloured area).

Figure 6.5: Two similar model views of a treatment plan for a prostate patient with and without the bone structure. The red circle indicates the gantry motion around the patient, the red bars are the control points. The yellow lines illustrate the beam at a specific position with the MLCs visible (Cancertype: Prostate, Patient ID: Prost19).

Chapter 7

Dosimetric Evaluation

7.1 Dose Volume Histogram

A dose volume histogram (DVH) is a way to illustrate the cumulative 3D dose distribution in 2D. The DVH allows the observer to investigate the total volume that receives a specific dose [13]. DVHs are used routinely for clinical evaluation of the dose distributions.

The DVH provides an overview of the entire dose distribution of a delineated structure in a single plot. By use of the DVHs, it is possible to evaluate the dose distribution in different regions of interest. However, a DVH does not provide any spatial information regarding the dose distribution.

The dose distribution can be shown as a differential and a cumulative DVH (Figure 7.1). The differential DVH shows the volume that receives a dose in a specific dose interval as a function of dose, and therefore visualizes the variation in dose over a given volume, as displayed in Figure 7.1(a). The corresponding cumulative DVH shows the volume of a structure that receives a certain dose or higher [27, p 423]. In Figure 7.1(b) it is seen that, 80 % of the medulla volume receives 50 % or more of the prescribed dose (100%).

Of the two types of DVH, the cumulative DVH is found to be the most useful

[27, p. 423]. The cumulative DVH will be referred to as DVH in the following.

Based on the DVH it is also possible to investigate if the dose is uniform throughout the target volume. The uniformity is seen when a large percentage of the volume receives a similar dose. The uniformity is displayed in the DVH as a steep slope. In Figure 7.1(b) it is seen that the PTV has a higher uniformity than medulla. The DVH for OARs should preferable have a concave appearance indicating that the OARs receive minimum dose [33, p. 722-724]. The ideal DVH is displayed in Figure 7.2, where the entire target will receive an uniform dose and the OAR will not receive any dose.

The dose distribution can be reported and compared by looking at some specific DVH points, in order to compare and evaluate the dose distributions based on the CT and the MR images. The DVH points are chosen in accordance with recommendations from the ICRU Report 83 [6].

For the PTV and the CTV, the following DVH points recommended:

- D_{median}: The absorbed dose received by 50 % of the volume.
- $D_{98\%}$: The near minimum absorbed dose that covers 98 % of the volume.
- $D_{2\%}$: The near maximum absorbed dose that covers 2 % of the volume.

$D_{98\ \%}$ has been chosen since it can be used to determine if there are low-dose areas present in the target volumes. In situations where $D_{98\ \%}$ is lower than the tolerance level, it should be investigated if the low-dose areas are in the centre of the target volume or at the boundary. Low-dose areas at the boundaries of the target volume are less critical.
$D_{2\ \%}$ is a more clinical relevant alternative to the maximum dose absorbed by the target volume.
D_{median}, has been chosen since it describes the typically absorbed dose in a homogeneous irradiated target volume. Additionally, the steepest slope in the DVH is often close to the median. The D_{median} therefore describes the most uniform absorbed dose [6].

The recommended absorbed dose values for the OAR are often the maximum absorbed dose value (D_{max}) for the serial organs and the median absorbed dose value (D_{median}) for the parallel organs. However, the DVH points used for the comparison of the dose distributions in the OAR will be introduced in Chapter 9, since they depend on the diagnostic group.

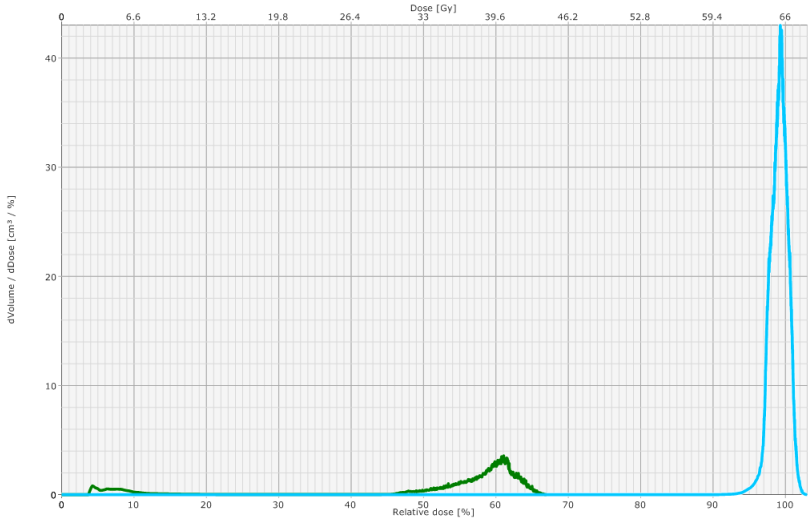

(a) Differential dose volume histogram

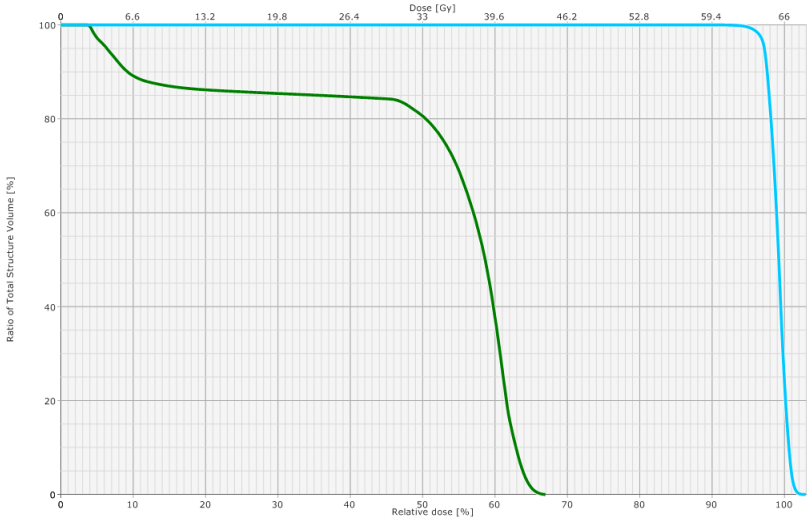

(b) Cumulative dose volume histogram

Figure 7.1: Dose Volume Histograms for medulla (green) and the PTV (blue). (Cancertype: Head & Neck, Patient ID: HN23).

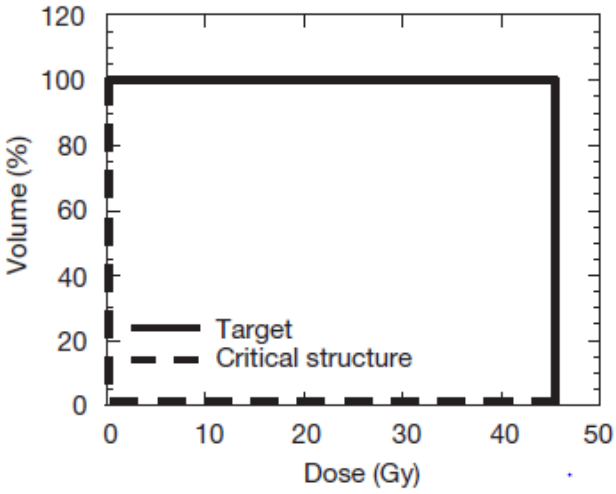

Figure 7.2: The ideal cumulative DVH. The entire target volume only receives the prescribed and the OAR (Critica structure) receives zero dose [42, p. 260].

7.2 Gamma Index Investigation

The gamma index is a quantity used to compare two dose distributions. The evaluation is based on a pass-fail criteria, where the predefined acceptance values for the distance to agreement (DTA) and the dose difference between the compared points must be meet. The gamma evaluation was presented by Low et al. and is based on a comparison of the calculated dose distribution (D_c) and the measured dose distribution (D_m). D_m is used as the reference [31].

This study utilizes the evaluation method in order to compare a CT-based dose distribution (which is used as the reference) with a dose distribution based on a density corrected MRI. The investigation is performed for each point (r_m) in the CT-based dose calculation, in order to find the most similar point (r_c) in the dose calculation based on the density corrected MRI. A passing criteria is set for both the DTA (measured in mm and denoted $\Delta\, d_M$) and the dose difference (measured in % and denoted $\Delta\, D_M$) [31].

Each point in the CT-based dose distribution, will have a corresponding gamma index, which can be found as [31]:

$$\gamma(r_m) = \min\{\Gamma(r_m, r_c)\}\forall\{r_c\} \tag{7.1}$$

where

$$\Gamma(r_m, r_c) = \sqrt{\frac{r^2(r_m, r_c)}{\Delta d_M^2} + \frac{\delta^2(r_m, r_c)}{\Delta D_M^2}} \tag{7.2}$$

The DTA is $r(r_m, r_c) = |r_c - r_m|$
and $\delta(r_m, r_c) = D_c(r_c) - D_m(r_m)$ describes the dose difference in each point when comparing a dose distribution based on the CT with a dose distribution based on the density corrected MRI.

The pass-fail criteria of gamma is:
$\gamma(r_m) \leq 1$, calculation passes
$\gamma(r_m) > 1$, calculation fails

If the dose difference and DTA are smaller than the acceptance criteria, it is seen that Equation 7.2 will be smaller than 1 and the calculation passes the pass-fail criteria.

Gamma Volume Histogram

Spezi et al. have extended the concept of the gamma evaluation, in order to provide a 3D measure of agreement between two dose distributions [47]. For each slice in the 3D volume a gamma map is calculated (see Figure 7.3(a)). The gamma map can be expressed as a cumulative histogram, denoted gamma area histogram (GAH), which is displayed in Figure 7.3(b). The GAH provides information regarding the percentage of an area which is described by a specific gamma value. Based on the GAHs a gamma volume histogram (GVH) can be obtained. The GVH describes the gamma values relative to the investigated volume [47], as displayed in Figure 7.3(c).
The GVH does not provide any spatial information concerning the difference in the dose distributions, as is also the case for the DVH. However, when investigation the GAHs it is possible to determine how large a percentage of the investigated area that fulfils the criteria in each slice of the investigated volume. The gamma evaluation is limited to points enclosed by the volume of interest. In our study the investigated volume is the PTV.

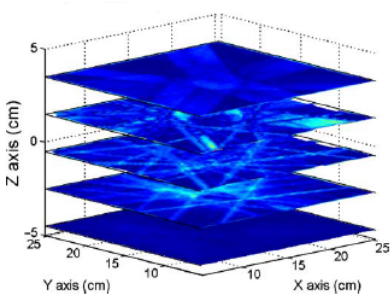

(a) 2D gamma maps

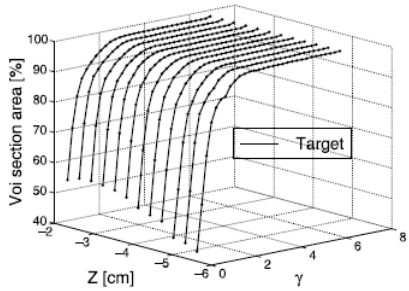

(b) Gamma area histograms

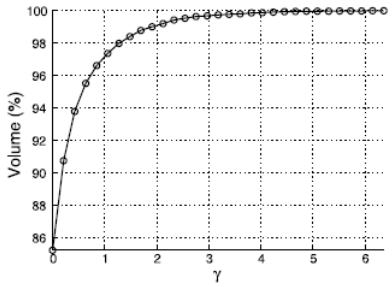

(c) Gamma volume histogram

Figure 7.3: The gamma maps and corresponding GAH describe the similarity in each slice of the investigated volume. The GVH displays the percentage of the investigated volume that corresponds to a specific gamma value [47].

Chapter 8

Materials & Methods

8.1 Data Specification

Our study is retrospective and includes data from 12 HN patients treated with static IMRT, 6 sarcoma (extremities only) patients treated with 3D CRT, 21 prostate and 5 pelvic (not prostate) patients treated with VMAT.

The data from each patient includes:

- CT scan + structure set
- T2 weighted MRI
- Clinically approved treatment plan

Each patient has a structure set, which contains information about all annotated structures including a full CT-based body outline.

The CT data is obtained with a Phillips Big Bore CT, while a 1T Panorama Phillips has been used to obtain the MRI data. The treatment planning software is Eclipse v.10.0 (Varian Medical Systems). The data set from each patient is

anonymized using ConQuest Dicom Server 1.4.15 and imported to Eclipse that is installed in a stand alone system (the T-box), which is not connected to the clinical system. The statistic analysis of the results has been performed with the statistical software *"R"* Version 2.11.0.

8.2 Data Processing

The aim of this study is to compare dose distributions based on different image modalities, as mentioned in the introduction.

The body outline is included separately in the CT- and MR images since the source-to-skin distance (SSD) is used in the dose calculation. Additionally, the body outline that is delineated on the MRI will contain geometrical distortion and is included in the MRI-based dose calculation. The remaining clinically approved structures are transferred from the CT to the MRI, in order to assign densities and compare dose to the target volumes and the OARs.

The dose calculation based on the MRI is evaluated in two different ways: 1) A homogeneous density assigned MRI (MRI_u), where the entire body is assigned a HU equal to water. 2) A heterogeneous density assigned MRI (MRI_b) where the CT segmented bone is transferred to the MRI and assigned an age dependent HU based on electron densities from the ICRU Report 46 [38] and the CT calibration curve (described in Section 4.1). The density corrected MRIs will be referred to as MRI_u and MRI_b in this study. The MRI_u and MRI_b are compared to the clinically approved dose distribution based on a CT.

Image Registration

When the data from the clinical system is imported to the T-box, the registration information is not transferred. Therefore, a registration of the MRI and the CT is performed. First part of the registration is performed manually, where the user moves the MRI in order to make a gross match to the CT. The matching is done three-dimensionally (axial, coronal and saggital), where the user is able to rigidly translate and rotate the MRI.

The manual registration is performed with the focus on different anatomical structures dependent on the diagnostic group. For the sarcoma and HN patients, the registration is primarily based on the bone structure where e.g. the prostate patients have gold seeds inserted to the prostate. The gold seeds will appear

bright in the CT images because of a high density and dark in the MR images, due to a low PD which results in loss of signal [41] (see Section 4.2). The image registration for prostate patients is primarily performed with regard to the gold seeds, since the prostate moves dependent on rectal and bladder filling [8].

After manually matching the two image modalities, a fine match is performed using an automatic 3D rigid registration. The registration is performed within a predefined volume of interest (VOI). In a rigid image registration, the geometrical match is based on translation and rotation of the template image. It is not possible to correct for deformation, since it is a 3D rigid registration algorithm [30, p. 19].

During the optimization of the 3D rigid registration a cost function is evaluated. The cost function is based on a similarity measure and the registration proceeds until the cost function is minimized, which corresponds to the maximum similarity. Since the algorithm can register a CT with an MRI, the similarity measure is expected to be mutual information. In Figure 8.3, a registered MRI and CT are displayed in a chess view.

Creating Bulk and Unit Density Assigned MRI

The MR images do not contain any information regarding the electron density of the tissues. Information regarding the attenuation of the beam is necessary in order to calculate the dose distribution in the TPS. This information is related to the electron density in the tissue. It is therefore necessary to assign a HU to the MR image. The HU is based on the CT calibration curve (see Section 4.1) and the electron densities from the ICRU Report 46 [38].

To calculate the dose distribution, it is also necessary to know the SSDs. Therefore, the patient body outline must be determined in the MRI. The body outline in the MR images are found by applying a pixel threshold to the image, based on a visual inspection of the pixel values. An example of the result of the pixel threshold is displayed in Figure 8.2(a). The pixel threshold is followed by a morphological closing. Last, the body outline is manually examined and adjustments are made slice-by-slice if necessary. In Figure 8.2(b) the result of the delineation of the body outline is shown.

For the $\mathrm{MRI_u}$ (Figure 8.3(a)), all tissues within the body outline are assigned an electron density equal to water (Section 4.1). The assumption is based on the knowledge that the body consist of 75 % water [34, p. 31]. This approach requires minimal image modification, and will be the simplest possible solution to calculate an MRI-based dose distribution. However, this assumption may

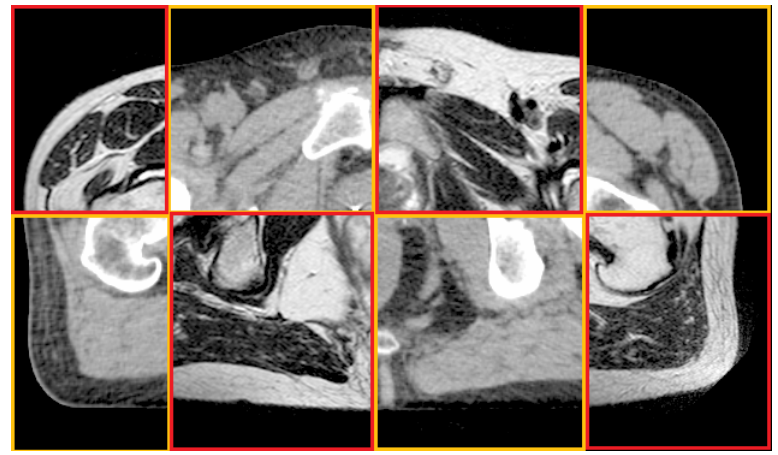

(a) Axial

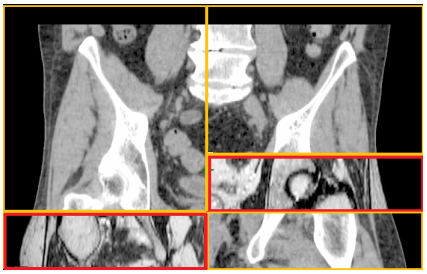

(b) Coronal

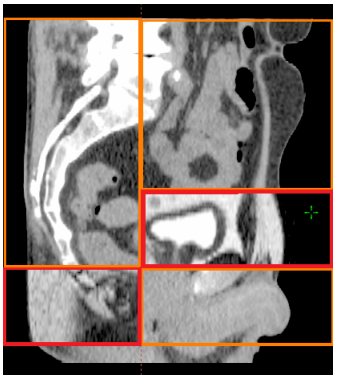

(c) Sagittal

Figure 8.1: A registered CT and MRI seen in a chess view. The orange squares are the CT and the red squares are the T2 weighted MRI (Cancertype: Prostate, Patient ID: Prost19).

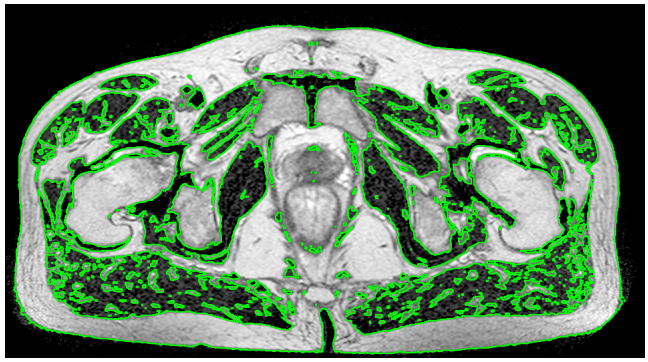

(a) The result of the pixel threshold

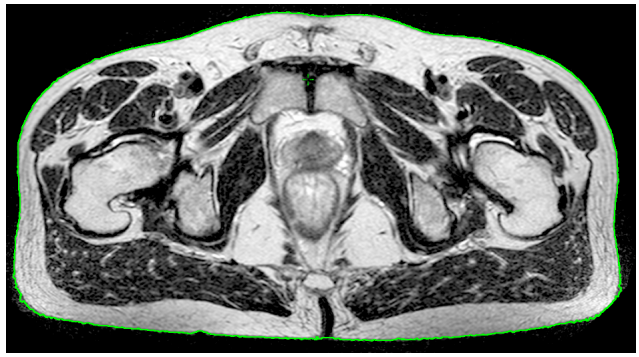

(b) After post processing

Figure 8.2: The body outline in the MRI is found with a pixel threshold followed by a morphological closing and manual corrections (Cancer-type: Prostate, Patient ID: Prost19).

not be reasonable, due to the high electron density in bone and a low density in the air cavities. A second approach, MRI_b, is therefore investigated. In MRI_b (Figure 8.3(b)) bone is assigned an electron density based on the specific bone tissue type and the remaining soft tissue is assigned the electron density equal to water. It is currently not possible to segmentate bone in the MR image, caused by the poor bone definition (see Section 4.2). Therefore, the bone segmentation is based on the CT information. In the CT image, bones are contoured using an automatic segmentation wizard in the TPS.

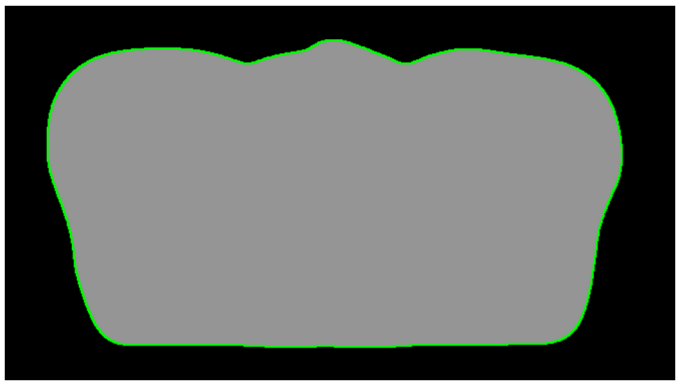

(a) MRI_u

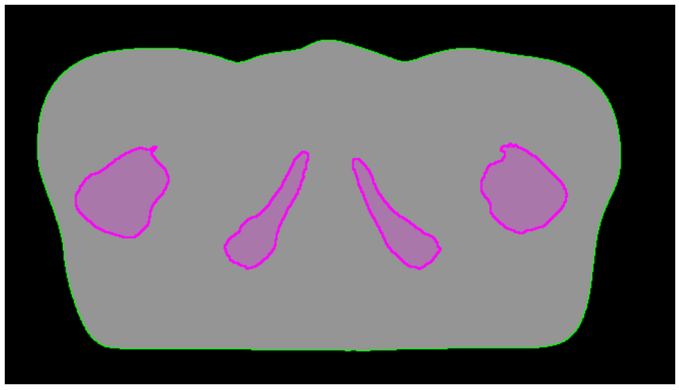

(b) MRI_b

Figure 8.3: In the MRI_u the entire body is assigned a HU equal to water (grey area). In the MRI_b the bone is assigned an age dependent HU, and the remaining tissue is assigned a HU equal to water (Cancertype: Prostate, Patient ID: Prost11).

For each diagnostic group, a HU has been calculated based on the representative bone tissue type. For prostate and pelvic patients the representative bone tissue

is femur. The electron density of femur decreases with age. Therefore the age dependent electron densities, according to ICRU Report 46 [38] are interpolated in order to find the appropriate electron density that corresponds to the average age of the two diagnostic groups. For each sarcoma patient, an individual HU is calculated, due to differences in electron densities for the bone tissue in the extremities. The calculation is based on the age and the bone tissue type of each sarcoma patient. For the HN patients, the HU is based on electron density information for skeleton cranium, which is not age dependent. The electron density and the calculated HU are listed for each diagnostic group in Table 8.1.

Table 8.1: Calculated HU.

Diagnostic Group	**Bone tissue**	**Electron density** ($g \cdot cm^{-3}$), ρ	**Calculated HU (age)**
HN	Skeleton-cranium(whole)	1.61 (adult) *	971
Prostate	Skeleton-femur(whole)	1.33 (30 years) 1.22 (90 years)	349 (66.8 years**)
Pelvic	Skeleton-femur(whole)	1.33 (30 years) 1.22 (90 years)	356 (64.7 years**)
Sarcoma			
Patient ID: Sar 1	Skeleton-cortical	1.92 *	1520
Patient ID: Sar 3	Skeleton-femur	1.33 (30 years) 1.22 (90 years)	332 (72 years)
Patient ID: Sar 5	Skeleton-femur	1.33 (30 years) 1.22 (90 years)	432 (42 years)
Patient ID: Sar 7	Skeleton-humerus	1.46 *	703
Patient ID: Sar 12	Skeleton-femur	1.33 (30 years) 1.22 (90 years)	292 (84 years)
Patient ID: Sar 15	Skeleton-cortical	1.92 *	1520

∗ Not age dependent.
∗∗ The average age in the diagnostic group.

A second approach to MRI_b is investigated, where air cavity is taken into consideration in addition to bone and soft tissue. The bulk density corrected MRI with the air cavity segmentation will be referred to as $MRI_{b,c}$ in this study. In the air cavities, the beam will hardly not be attenuated, which will poten-

tially lead to an error in the calculation of the dose distribution when assuming that air cavities correspond to water. In order to overcome this, air cavities are segmented with the same method as was described for delineation of the body outline. The segmented air cavities are assigned the HU corresponding to air (HU = -1000 [11, p. 356]). This approach is only found necessary for the HN patients, therefore the $MRI_{b,c}$ is investigated for this specific group.

All the CT structures, except for the body outline are transferred to the MRI. For some patients, the target volumes from the CT will exceed the body outline of the MRI. In these situations the target volumes will be cropped, with a margin of 3 mm, to fit the body outline of the MRI. This approach was necessary for the PTV from 4 HN patients, and the PTV and the CTV from 5 and 3 sarcoma patients, respectively.

Calculation of Dose Distribution

The CT-based clinical treatment plan and the structure set are registered to the corresponding density corrected MRIs. The dose distributions are calculated for the density corrected MRIs and the CT, with fixed MUs from the original CT-based treatment plan. The 3D dose distributions can be evaluated based on a visual inspection. Additionally, the TPS gives the opportunity to evaluate the dose distributions with use of the DVHs (See section 7.1). The DVH points recommended by the ICRU Report 83 [6] are used to compare the dose distributions based on the density corrected MRIs and the CT.

8.3 Statistical Analysis of Dose Volume Histogram Points

A statical analysis is used to evaluate the density corrected MRIs in a comparison to the CT. The statistical analysis is performed individually on each diagnostic group for a number of reported DVH points.

The procedure of the statistical analysis is exemplified for a comparison of the PTV $D_{98\%}$ for the prostate group. The investigated DVH is displayed in Figure 8.4.

In Figure 8.5, the data for PTV $D_{98\%}$ is summarised in a box- and whisker plot. The box- and whisker plot illustrates the quartiles in the data where each quartile describes 25 % of the data. The box illustrates the 2nd and 3rd quartile,

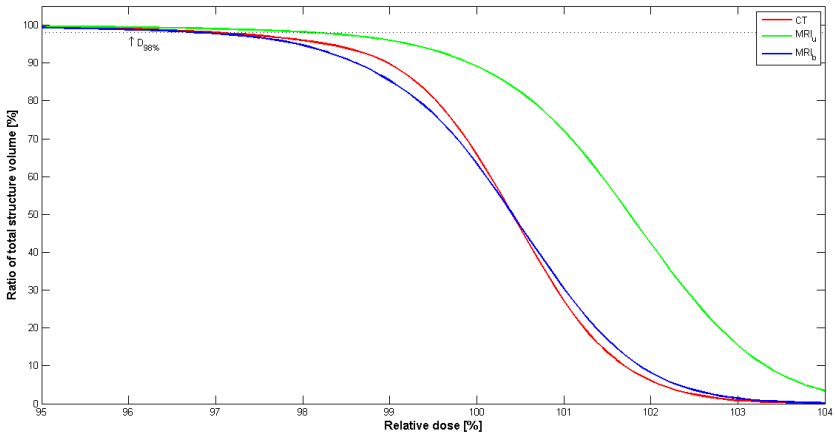

Figure 8.4: The average DVHs are based on 21 prostate patients, with the investigated DVH point, PTV $D_{98\%}$.

which are separated by the median [35, p. 54]. The whiskers indicate the 1st and 4th quartile and extends to the minimum and the maximum value, respectively. However, the whiskers only extend to the smallest/largest observation when it is not to far from the 2nd/3rd quartile (the observation must be within 1.5 $\times$ the interquartile range). Data points that do not fulfil these criteria are displayed as outliers [24, p. 35].

In Figure 8.5, it is seen that the median in the data seems to be similar for CT and the MRI_b, and that the variation in the data from the the two density corrected MRIs are similar.

In order to determine if the investigated DVH points calculated based on the density assigned MRIs and CT have equal means an one-way two tailed ANOVA is performed. Prior to the ANOVA, assumptions about the data must be fulfilled, i.e. the data must be normally distributed with equal variances [24, p. 404-405].

These assumptions are investigated in Figure 8.6. Figure 8.6(a) and Figure 8.6(c) are used to evaluate the constancy of the variances. To assume that the variances are constant, no trend should be seen and the red line should be nearly horizontal [35, p. 142]. A nearly horizontal line is seen in both Figure 8.6(a) and Figure 8.6(c), therefore the variances are assumed to be constant.

Figure 8.6(d), illustrates the leverage, which is the influence of each observation.

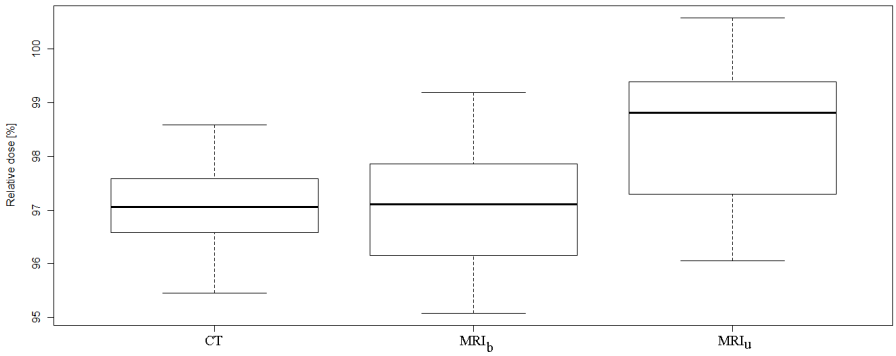

Figure 8.5: A box- and whisker plot for PTV $D_{98\%}$.

The influence increases if outliers are present in the data [35, p. 123]. The red line would ideally be a straight horizontal line, which indicates that there are no distortion of the parameter estimates due to highly influential values [36, p. 458]. In Figure 8.6(d) the red line is nearly a straight horizontal line, and no parameter distortion is therefore expected.

Figure 8.6(b) is used to compare two probability distributions, by plotting their quantiles against each other. The ordinate shows quantiles of the residuals from the sample data and the abscissa shows quantiles from a standard normal distribution. If the two distributions are similar, the points in the quantile-quantile (QQ) plot will be linear related, indicating that the sample data follows a normal distribution [49]. The residuals seen in the QQ-plot in Figure 8.6(b) are linearly related, based on this the residuals are assumed to be normally distributed.

The normality of the data is further investigated using the Shapiro-Wilks normality test, which tests the null-hypothesis that a sample is normally distributed. When the p-value is less than .05, the data is taken to be significantly different, and the null hypothesis is rejected. With a p-value of more than .05, the data are taken to be non-significant, and the null hypothesis cannot be rejected [24, p. 409-410]. The significance describes how likely it is that a result has occurred by chance, if the null hypothesis is true. The p-value is a measure of the credibility of the null hypothesis [35, p. 3-4]. For the PTV $D_{98\%}$, the p-value from the Shapiro-Wilks normality test has been determined to 0.31, and the null hypothesis cannot be rejected with a significance level of .05. The data is therefore assumed to be normally distributed. Since the assumptions are

reasonable fulfilled for the PTV $D_{98\%}$ an ANOVA is performed.

The null hypothesis and the alternative hypothesis can be written as [24, p. 410]:

$$H_0 : \mu_{\mathrm{CT}} = \mu_{\mathrm{MRI_u}} = \mu_{\mathrm{MRI_b}}$$

$$H_1 : \mu_{\mathrm{CT}} \neq \mu_{\mathrm{MRI_u}} \neq \mu_{\mathrm{MRI_b}}$$

The result from the ANOVA of the PTV $D_{98\%}$ for the prostate patients gives a p-value of $2.3{\cdot}10^{-4}$. The null hypothesis can therefore be rejected, which means that the investigated DVH points cannot be considered to have equal means.

The data is investigated further using a paired t-test. The paired t-test is chosen since the CT- and MRI-based dose distributions are calculated on the same patient, therefore correlation must be taken into consideration. In the paired t-test the CT is compared to the $\mathrm{MRI_u}$ and the $\mathrm{MRI_b}$, respectively. Additionally, the $\mathrm{MRI_u}$ and the $\mathrm{MRI_b}$ are compared. The null and the alternative hypothesis are as follows [24, p. 261]:

$$H_0 : \mu_{\mathrm{CT}} = \mu_{\mathrm{MRI_u}},\ H_1 : \mu_{\mathrm{CT}} \neq \mu_{\mathrm{MRI_u}}$$

$$H_0 : \mu_{\mathrm{CT}} = \mu_{\mathrm{MRI_b}},\ H_1 : \mu_{\mathrm{CT}} \neq \mu_{\mathrm{MRI_b}}$$

$$H_0 : \mu_{\mathrm{MRI_u}} = \mu_{\mathrm{MRI_b}},\ H_1 : \mu_{\mathrm{MRI_u}} \neq \mu_{\mathrm{MRI_b}}$$

The results of the paired t-test are displayed in Table 8.2. The $\mathrm{MRI_u}$ differs significantly from both the $\mathrm{MRI_b}$ and the CT. Additionally no significant difference are found when comparing the $\mathrm{MRI_b}$ and the CT. It can therefore be concluded that there is no difference in means between the $\mathrm{MRI_b}$ and the CT for the investigated DVH point.

Table 8.2: The result of the paired t-test for PTV $D_{98\%}$

Comparison	P-value	Significant
CT vs. $\mathrm{MRI_u}$	$2.7 \cdot 10^{-3}$	S
CT vs. $\mathrm{MRI_b}$	0.87	NS
$\mathrm{MRI_u}$ vs. $\mathrm{MRI_b}$	$2.2 \cdot 10^{-16}$	S

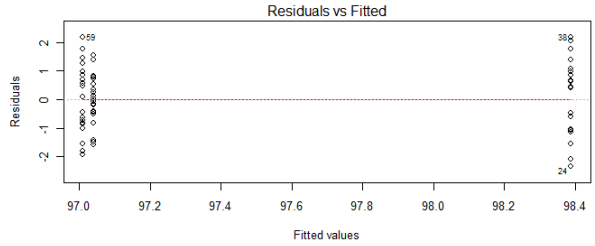

(a)

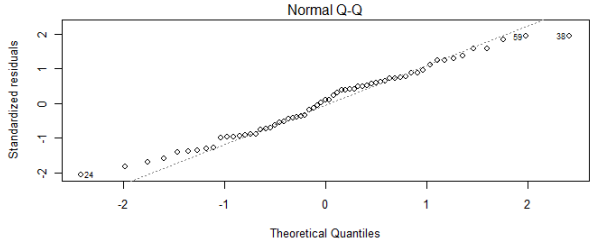

(b)

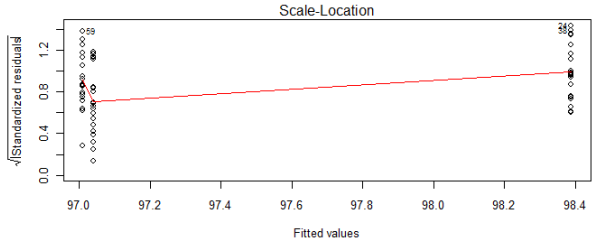

(c)

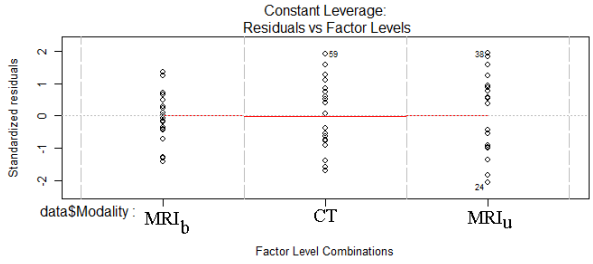

(d)

Figure 8.6: Statistical diagnose plots for PTV $D_{98\%}$.

8.4 Gamma Volume Histogram Analysis

The gamma volume histogram (GVH) is used to evaluate the dosimetric differences of the dose distributions calculated based on the density corrected MRIs and the CT, respectively. The calculated dose distributions are exported from the TPS and imported into the computational environment for radiotherapy research (CERR), which is a MATLAB based software [1]. The gamma evaluation is afterwards performed using the DICOM-RT-based toolbox, which was developed by Spezi et al. for the evaluation and verification of radiotherapy treatment plans. The toolbox contains a set of functions written in MATLAB [48].

The treatment plan and the corresponding dose distribution for the CT and the density corrected the MRIs, as well as the CT-based structure set are exported and analysed in MATLAB using the DICOM-RT-based toolbox. Based on the information in the structure set, it is possible to evaluate different structures individually. The process is summarized in Figure 8.7.

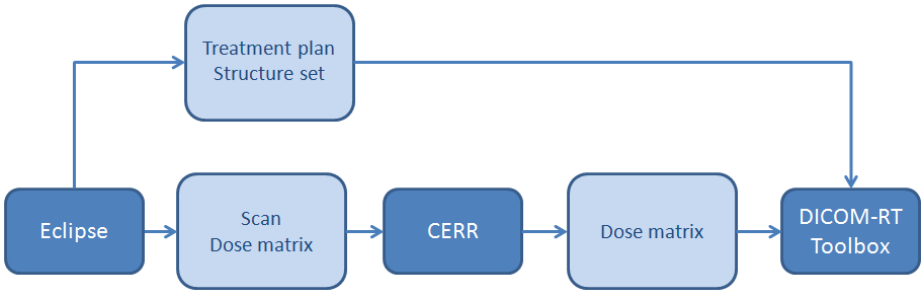

Figure 8.7: Preparing data for the the gamma evaluation. The data is exported from Eclipse and evaluated with the DICOM-RT Toolbox.

In our study, a gamma evaluation is performed of the PTV for 20 prostate patients (1 prostate patient is excluded from the evaluation, due to a irrecoverable loading error of the structure set). The CT-based dose calculation is compared to the dose distribution based on the density corrected MRIs. The dose distributions calculated based on the density corrected MRIs are linearly interpolated in the z-direction, prior to the gamma evaluation. This is done in order to create a resolution that corresponds to the CT-based dose distribution. The registration information obtained from the TPS, regarding the translation is applied to the MRI, in order to obtain a comparable coordinate system. In the registration information the rotation were found to be less than 1 degree in all directions for the majority of patients. Therefore, the rotation information is not considered. The dose distributions based on the CT and the density corrected MRIs are cropped to achieve comparable dimensions. The gamma evaluation is per-

formed on each slice of the PTV, and the results are summarised in a GVH, see Section 7.2.

The investigation is performed with 3 combinations of acceptance criteria (DTA / dose difference):

- $\gamma_{2\text{mm}/2\%}$
- $\gamma_{2\text{mm}/3\%}$
- $\gamma_{3\text{mm}/3\%}$

Figure 8.8 illustrates a 2D dose distribution in the corresponding slices. The figure includes the body outline and the PTV. The gamma evaluation is performed on PTV. Figure 8.9(b) illustrates the resulting gamma map. The information from the gamma map is summarised in a gamma histogram, which is displayed in Figure 8.9(c). There is a large resemblance between the dose distribution based on the CT and the MRI_u in the investigated slice. The gamma map is generated for each slice of the PTV and is represented as a GVH, as is displayed in Figure 8.10. The relation between the percentage volume of the PTV covered by a specific gamma value or less is described by the GVH. In Figure 8.10 the percentage volume of the accepted gamma values is 85 %.

The accepted percentage volume of the PTV ($\gamma \leq 1$) is used to perform a statistical analysis. The statistical analysis is performed with a paired t-test in a similar procedure as described in Section 8.3.

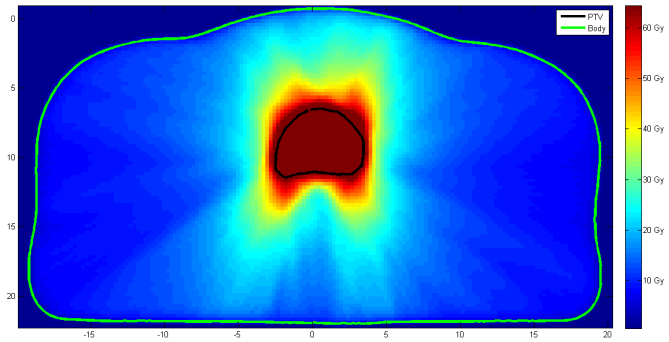

(a) Dose distribution calculated based on CT, including the body outline and the PTV

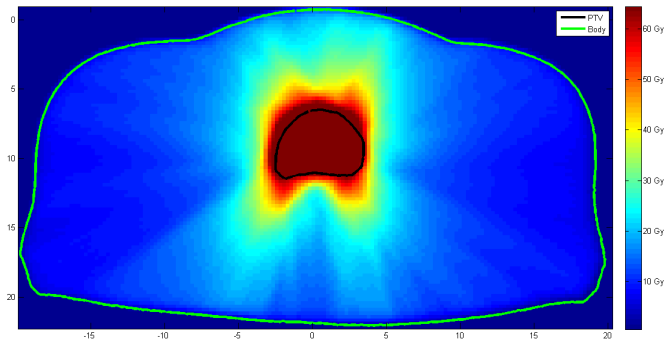

(b) Dose distribution calculated based on MRI_u, including the body outline and the PTV

Figure 8.8: A 2D comparison of dose calculations based on the CT and the MRI_u. z = -2.6 (Cancertype: Prostate, Patient ID: Prost38).

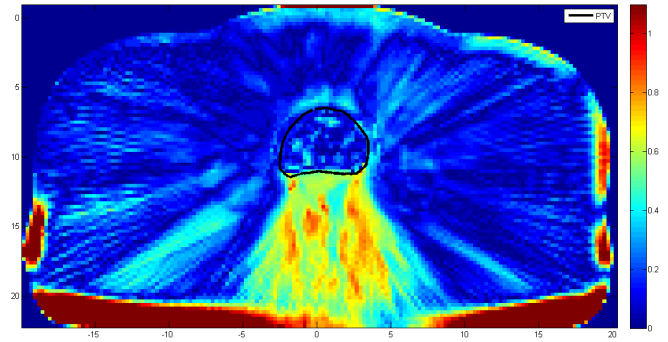

(a) Gamma map with the countour of the PTV

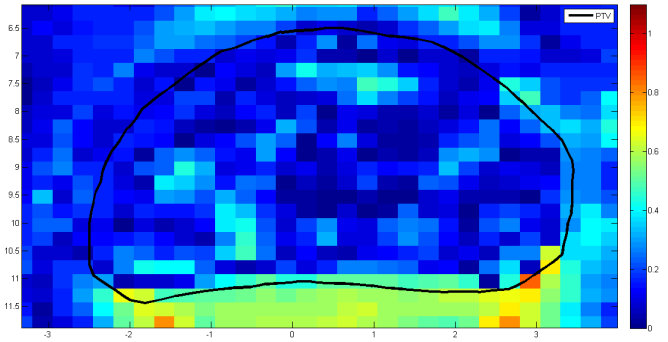

(b) Extraction of the gamma map above

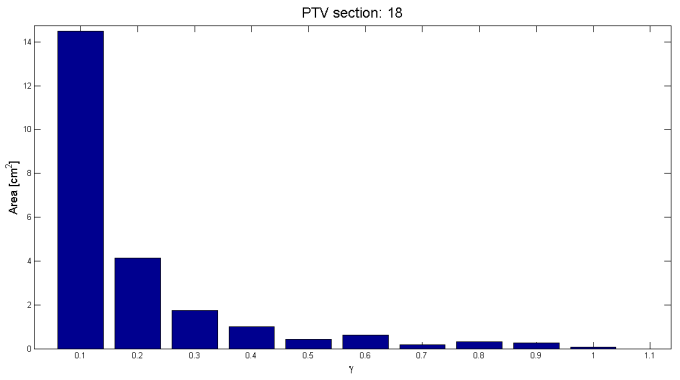

(c) Gamma histogram

Figure 8.9: The result of the 2D comparison of the dose calculations based on CT and MRI_u. The acceptance criteria $\gamma_{3mm/3\%}$ is used, z = -2.6 (Cancertype: Prostate, Patient ID: Prost38).

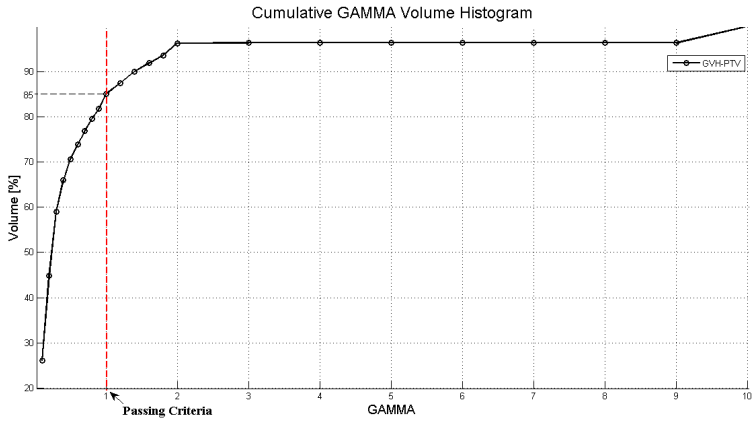

Figure 8.10: A GVH describing the similarity in dose distributions calculated based on the CT and the $\mathrm{MRI_u}$, respectively. The evaluation is performed for the PTV with the gamma criteria $\gamma_{3\mathrm{mm}/3\%}$ (Cancertype: Prostate, Patient ID: Prost33).

Chapter 9

Results of Dose Volume Histogram Analysis

9.1 Statistical Analysis of Dose Volume Histogram Points

Each diagnostic group is investigated in order to determine if the data is normally distributed. This is firstly done with the Shapiro-Wilks normality test, furthermore, the data is evaluated with box- and diagnostics plots. Some of the data appears to contain outliers. The outliers are not removed since they are caused by the clinical variation and not errors in the data processing. When evaluating the data using the Shapiro-Wilks normality tests and the QQ-plots it is found that the majority of the data are normally distributed. Taking into consideration that the samples are relatively small, and therefore more sensitive to variation, the data which is not normally distributed, is found to be approximately normal distributed. From the box- and diagnostics plot it is found that data have equal variances. Therefore the data for all diagnostic groups fulfil the criteria for the ANOVA.

Recommended absorbed dose values (defined in Section 7.1), are tested with the ANOVA. The results of the ANOVA are shown with a p-value indicating the significance/non significance. For each comparison, a percentage difference is

calculated based on the mean value, and the result is given with ± two standard deviations of the percentage difference.

The target volumes, PTV and CTV, will be used for the statistical analysis of all the diagnostic groups. The OAR differs dependent on the diagnostic groups, and the DVH points will therefore be introduced with the diagnostic group.

9.1.1 Head & Neck Patients

For the head & neck patients, the differences in dose distributions based on density corrected MRIs (MRI_u, MRI_b, $MRI_{b,c}$), and CT are quantified using DVH points. The reported dose values for the OAR are based on the clinical guidelines recommended in DAHANCA (2004) [16]:

- Medulla: The maximum dose D_{max}
  Constraint: 45 Gy
- Brain stem: The maximum dose D_{max}
  Constraint: 45 Gy
- Parotid: The mean dose D_{median}
  Constraint: 26 Gy
- Larynx: 2/3 of the volume $D_{2/3\ Vol.}$
  Constraint: 50 Gy

The number of patients in Table 9.1 vary for the structures, since the diagnostic group contains different differential diagnoses.

The results are shown in Table 9.1. None of the parameters are significantly different when comparing the CT and the density corrected MRIs. The percentage difference in Table 9.1 show that the density corrected MRIs differ less from the CT in the target volumes than the OAR. Additional, the OARs have higher standard deviations than the target volumes.
Comparing the density corrected MRIs for the PTV and the CTV, it is seen that the MRI_u differs more from the CT than the MRI_b and the $MRI_{b,c}$, respectively. The bulk density corrected MRIs do not differ from each other, indicating that air segmentation does not contribute with results that are closer to the CT.

In Figure 9.1 the average DVHs for the PTV based on the 12 HN patients are displayed. The MRI_b and $MRI_{b,c}$ are more similar to the CT than the MRI_u, as displayed in Table 9.1. In a visual inspection of the PTV, it is found that the MRI_u gives a higher and less uniform dose, than the bulk density assigned MRIs.

Figure 9.2 illustrates the average DVH for medulla based on 12 HN patients. A visual inspection of the DVH for medulla shows that $MRI_{b,c}$ contributes with a dose to a larger relative volume. It is seen that 80 % of medulla receives 10 Gy or more with CT. With MRI_b and MRI_u will 83 % of medulla receive 10

Table 9.1: Statistical Results of Head & Neck Patients

Volume (number of patients)	DVH point	MRI_u[%]	MRI_b[%]	$MRI_{b,c}$ [%]	P-value	Significant
PTV(12)	D_{median}	1.0 ± 2.3	-0.6 ± 1.3	-0.3 ± 1.5	0.11	NS
	$D_{98\%}$	1.0 ± 5.8	-0.5 ± 5.4	-1.8 ± 5.1	0.23	NS
	$D_{2\%}$	1.0 ± 2.3	-0.6 ± 1.1	-0.1 ± 0.8	0.20	NS
CTV(12)	D_{median}	0.9 ± 2.3	-0.5 ± 1.7	-0.4 ± 1.6	0.32	NS
	$D_{98\%}$	-1.2 ± 4.2	-0.2 ± 3.7	-0.8 ± 4.2	0.10	NS
	$D_{2\%}$	1.1 ± 2.2	-0.5 ± 1.4	-0.2 ± 1.0	0.28	NS
Medulla(12)	Dmax	1.4 ± 11.6	-4.5 ± 12.8	-3.8 ± 11.8	1.0	NS
Brainstem(9)	Dmax	1.8 ± 12.6	-1.6 ± 11.8	-1.7 ± 11.9	1.0	NS
Parotid sin(11)	D_{median}	-3.9 ± 18.0	-5.1 ± 19.0	-4.5 ± 17.4	1.0	NS
Parotid dxt(11)	D_{median}	2.5 ± 29.3	1.0 ± 27.3	1.9 ± 29.8	1.0	NS
Larynx(7)	$D_{2/3\ Vol.}$	-2.0 ± 8.6	-2.5 ± 8.4	-2.0 ± 9.0	1.0	NS

* The percentage differences of the MRI_u, $MRI_b$and $MRI_{b,c}$ with respect to the CT in mean value ± two standard deviations.
Significance level $p<0.05$. NS = Not significant. S = Significant.

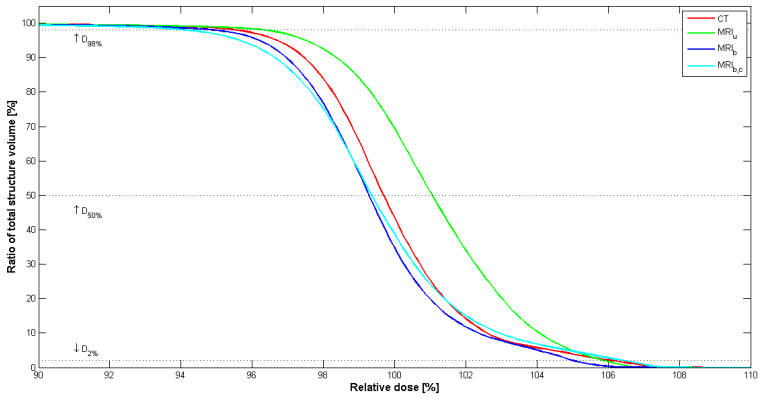

Figure 9.1: The average DVH for PTV based on 12 HN patients. The investigated DVH points are indicated.

Gy or more. For $MRI_{b,c}$, 88 % of medulla will receive 10 Gy or more. However, the investigated DVH point shows that D_{max} is 3.8 % smaller for $MRI_{b,c}$ than D_{max} calculated based on CT, as displayed in Table 9.1. Additionally, it is seen in Figure 9.2, that none of the investigated DVHs exceed the maximum recommended dose of 45 Gy to medulla.

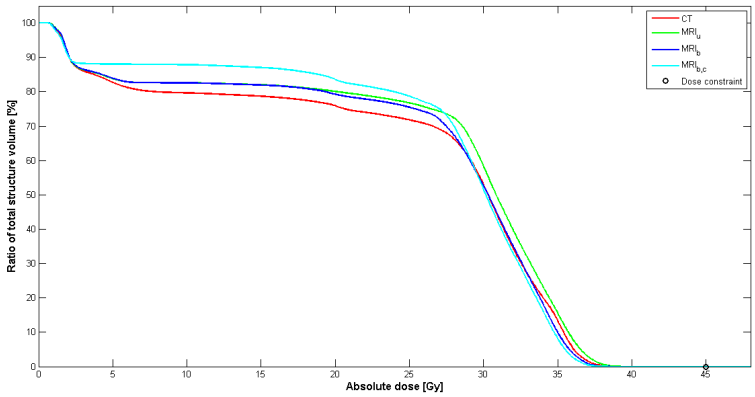

Figure 9.2: The average DVH for medulla based on 12 HN patients. The dose constrain is visualized as a circle.

9.1.2 Sarcoma Patients

The analysis for the sarcoma patients is based on 6 patients. The statistical analysis is only performed on the target volumes, since the sarcoma patients do not have comparable OAR.

The results in Table 9.2 show that none of the DVH points are significantly different when comparing the CT, MRI_u and the MRI_b. Based on the percentage differences it is seen that there is no distinct difference between the calculations based on the density corrected MRIs. $D_{98\%}$ are showing a high standard deviation for the target volumes, this is seen for both MRI_b and MRI_u.

Table 9.2: Statistical Results of Sarcoma Patients

Volume (number of patients)	DVH point	MRI_u [%]*	MRI_b [%]*	P-value	Significant
PTV(6)	D_{median}	-1.0 ± 1.8	-1.6 ± 3.0	0.63	NS
	$D_{98\%}$	-2.2 ± 19.1	-2.3 ± 19.2	0.64	NS
	$D_{2\%}$	-1.4 ± 3.2	-1.5 ± 3.6	0.35	NS
CTV(6)	D_{median}	-1.2 ± 2.3	-1.5 ± 2.8	0.70	NS
	$D_{98\%}$	-0.9 ± 17.7	-1.1 ± 17.3	0.81	NS
	$D_{2\%}$	-1.6 ± 3.7	-1.6 ± 3.7	0.30	NS

* The percentage differences of the density corrected MRIs with respect to the CT, in mean value ± two standard deviations. Significance level $p<0.05$.
NS = Not significant. S = Significant.

In Figure 9.3 the average DVHs for PTV are displayed. It is seen that there is a large resemblance between the DVHs.

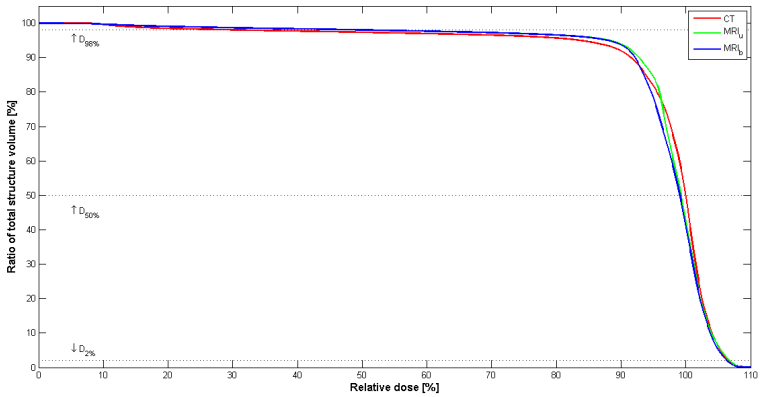

Figure 9.3: The average DVH for PTV based on 6 sarcoma patients. The investigated DVH points are indicated.

9.1.3 Pelvic Patients

For the pelvic patients the comparison of the DVHs for the OARs are based on guidelines from Herlev Hospital [5]. The following DVH points are used:

- Femur sin./dxt.: The mean dose D_{mean}
  Constraint: 33 Gy
- Femur sin./dxt.: The maximum dose D_{max}
  Constraint: 52 Gy

The percentage differences in the DVH points calculated based on the MRI_u, the MRI_b and the CT are similar as displayed in Table 9.3. The variation is similar for the targets and the OAR. The variation is in the range of [1.2,3.8] for the MRI_u and in the range of [1.5,2.6] for the MRI_b. The calculations based on density corrected MRIs do not differ significantly from the CT-based in the investigated DVH points.

The described similarities are also visualized in Figure 9.4 for the PTV and for femur dxt./sin. in Figure 9.5. The DVH describing the dose distribution in the PTV displays a higher uniformity for the CT-based calculations, than the calculations based on the density assigned MRIs.

Table 9.3: Statistical Results of Pelvic Patients

Volume (number of patients)	DVH point	MRI_u [%]*	MRI_b [%]*	P-value	Significant
PTV(5)	D_{median}	0.2 ± 1.5	-0.3 ± 1.6	0.53	NS
	$D_{98\%}$	-0.7 ± 2.3	-1.1 ± 2.0	0.36	NS
	$D_{2\%}$	0.6 ± 1.8	0.06 ± 2.1	0.50	NS
CTV(5)	D_{median}	0.3 ± 1.5	-0.1 ± 1.7	0.60	NS
	$D_{98\%}$	-0.3 ± 2.2	-0.7 ± 1.9	0.38	NS
	$D_{2\%}$	0.6 ± 2.0	0.1 ± 2.2	0.61	NS
Fem dxt.(5)	D_{mean}	-0.2 ± 3.8	0.09 ± 2.6	1.0	NS
	D_{max}	-0.2 ± 2.7	-0.7 ± 1.5	1.0	NS
Fem sin.(5)	D_{mean}	0.2 ± 1.2	-0.3 ± 1.5	1.0	NS
	D_{max}	0.003 ± 1.8	-0.5 ± 1.5	0.98	NS

* The percentage differences of the MRI_u and MRI_b with respect to the CT, in mean value ± two standard deviations.
Significance level $p<0.05$. NS = Not significant. S = Significant.

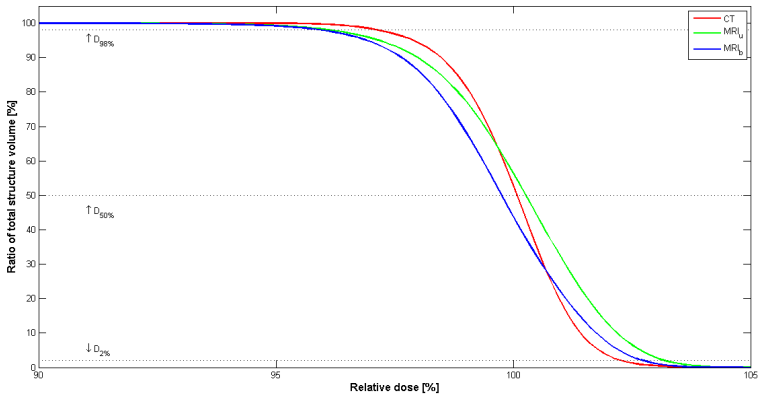

Figure 9.4: The average DVH for PTV based on 5 Pelvic patients. The investigated DVH points are displayed.

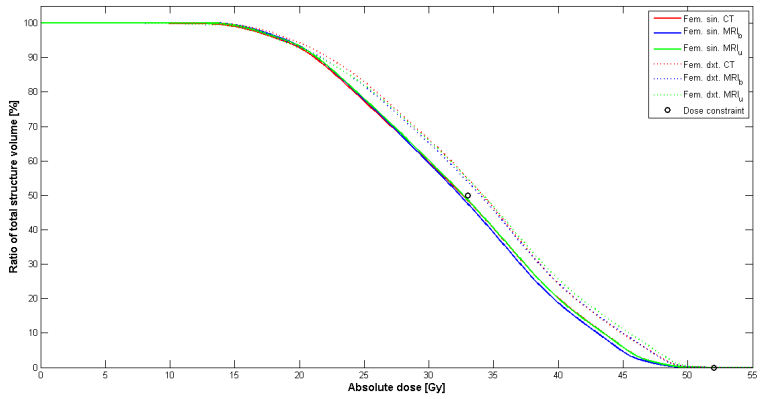

Figure 9.5: The average DVH for Femur dxt. and Femur sin. based on 5 Pelvic patients. The dose constrains are indicated.

9.1.4 Prostate Patients

For the prostate patients the DVH points used to compare the DVH for the OARs are based on clinical guidelines from Herlev Hospital [45].

- Rectum: The dose absorbed by 60 % of the volume $D_{60\ \%}$
  Prescribed dose of 70 Gy, constraint: 36 Gy
  Prescribed dose of 78 Gy, constraint: 40 Gy
- Rectum: The dose absorbed by 30 % of the volume $D_{30\ \%}$
  Prescribed dose of 70 Gy, constraint: 54 Gy
  Prescribed dose of 78 Gy, constraint: 60 Gy
- Rectum: The dose absorbed by 10 % of the volume $D_{10\ \%}$
  Prescribed dose of 70 Gy, constraint: 65 Gy
  Prescribed dose of 78 Gy, constraint: 75 Gy

During the investigation of the OAR, the prostate patients are separated since the dose constraints for rectum depend on the prescribed dose. 12 patients have a prescribed dose of 70 Gy, while the remaining 9 patients have a prescribed dose of 78 Gy.

The results are shown in Table 9.4. The statistical analysis shows that there is no significant difference for the OAR. The percentage difference between the CT

and the MRI_u is in the range of ± 2.2 % for the investigated DVH points. The MRI_b differs in the range of ± 0.9 %. It is difficult to differentiate between the CT and the density corrected MRIs in a visual inspection of the shape of the DVH (Figure 9.6). Furthermore, it is seen that the shape of the DVH depends on the prescribed dose. It is also investigated if the OAR could be evaluated as one group, without taking the prescribed dose into consideration. However it was found that this approach was not possible for the OAR, see Appendix C.

The results of the statistical analysis of the target volumes for the CT- and the two MRI-based calculations are displayed in Table 9.4. There is significant difference for all the target volumes. Therefore, a paired t-test is performed in order to investigate the differences in means further.

Table 9.4: Statistical Results of Prostate Patients

Volume (number of patients)	DVH point	MRI_u [%]*	MRI_b [%]*	P-value	Significant
PTV(21)	D_{median}	1.3 ± 1.4	-0.0002 ± 1.1	$2.2 \cdot 10^{-10}$	S
	$D_{98\%}$	1.4 ± 1.9	-0.03 ± 1.7	$2.3 \cdot 10^{-4}$	S
	$D_{2\%}$	1.4 ± 1.3	-0.02 ± 1.0	$2.4 \cdot 10^{-9}$	S
CTV(21)	D_{median}	1.3 ± 1.4	-0.005 ± 1.1	$3.4 \cdot 10^{-10}$	S
	$D_{98\%}$	1.4 ± 1.5	0.1 ± 1.3	$6.0 \cdot 10^{-9}$	S
	$D_{2\%}$	1.3 ± 1.4	0.1 ± 1.8	$6.0 \cdot 10^{-8}$	S
Rectum**(12)	$D_{10\%}$	2.0 ± 1.7	0.6 ± 1.6	0.26	NS
	$D_{30\%}$	1.9 ± 2.5	0.8 ± 2.5	0.87	NS
	$D_{60\%}$	1.0 ± 3.0	0.2 ± 3.0	0.97	NS
Rectum***(9)	$D_{10\%}$	2.2 ± 3.0	0.9 ± 3.0	0.80	NS
	$D_{30\%}$	0.8 ± 1.5	-0.008 ± 1.3	0.99	NS
	$D_{60\%}$	-0.006 ± 1.6	-0.7 ± 1.6	0.99	NS

* The percentage differences of MRI_u and MRI_b with respect to CT, in mean value ± two standard deviations. **For prostate patients with a prescribed dose of 70 Gy. ***For prostate patients with a prescribed dose of 78 Gy. Significance level $p<0.05$. NS = Not significant, S = Significant.

Calculations based on the MRI_u differs significantly from calculations based on both the CT and the MRI_b, as displayed in Table 9.5. At the same time no significant difference is seen when comparing calculations based on the CT and the MRI_b. The average DVH for the PTV is shown in Figure 9.7. A visual inspection of the average DVHs show that the MRI_b and the CT are similar in shape in contrast to the MRI_u, which gives a higher dose. The visual inspection support the results of the statistical analysis.

Table 9.5: The results of a paired t-test for comparison of calculations based on CT, MRI_u and MRI_b

Volume	DVH point	CT vs. MRI_u P-value	MRI_u vs. MRI_b P-value	CT vs. MRI_b P-value
PTV	D_{median}	$2.7 \cdot 10^{-3}$	$2.4 \cdot 10^{-16}$	1.0
	$D_{98\%}$	$2.7 \cdot 10^{-3}$	$2.2 \cdot 10^{-16}$	0.87
	$D_{2\%}$	$2.7 \cdot 10^{-3}$	$5.9 \cdot 10^{-14}$	0.87
CTV	D_{median}	$2.7 \cdot 10^{-3}$	$5.4 \cdot 10^{-16}$	0.97
	$D_{98\%}$	$2.7 \cdot 10^{-3}$	$3.3 \cdot 10^{-15}$	0.49
	$D_{2\%}$	$2.7 \cdot 10^{-3}$	$1.5 \cdot 10^{-14}$	0.50

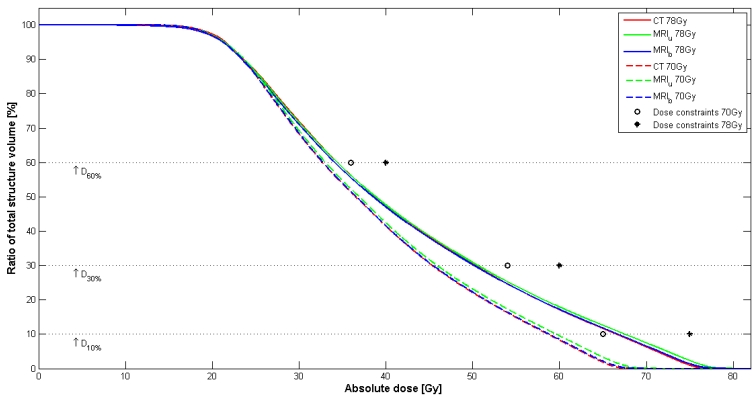

Figure 9.6: The average DVH for the rectum for 9 prostate patients with a prescribed dose of 78 Gy and 12 prostate patients with prescribed dose of 70 Gy. The constraints are visualized.

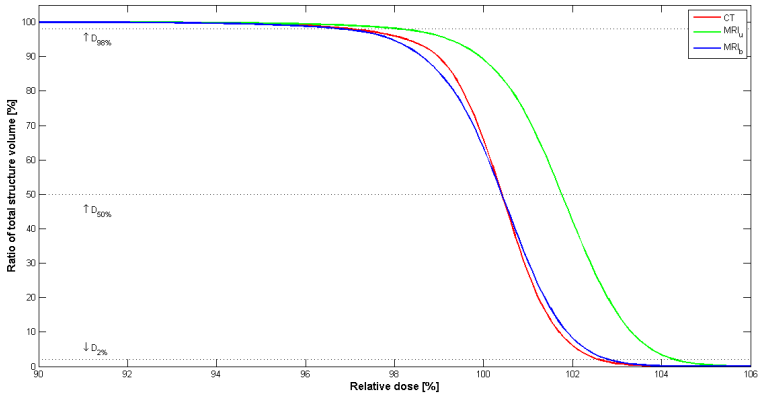

Figure 9.7: The average DVH for the PTV of 21 prostate patients. The investigated DVH points are indicated.

Chapter 10

Results of Gamma Index Investigation

10.1 Statistical Analysis for Gamma Volume Histograms

For the PTV of 20 prostate patients, a gamma investigation is performed and evaluated with a GVH. The compared dose distributions are calculated based on the CT, the MRI_u and the MRI_b. The evaluation of the relative volume which meets the acceptance criteria, is performed for 3 combinations of acceptance criteria ($\gamma_{2mm/2\%}$, $\gamma_{2mm/3\%}$, $\gamma_{3mm/3\%}$), as described in Section 8.4.

The data is investigated and is found to be normally distributed. Therefore, a paired t-test is used in the statistical analysis of the GVH points. In Table 10.1, the mean values and the range of the percentage of points in the PTV that fulfil the gamma criteria are displayed. The MRI_b is more similar to the CT than the MRI_u. In the statistical analysis, it is found that the comparison between the CT and MRI_b is significantly better than the comparison between the CT and the MRI_u, for all investigated combinations of the gamma criteria.

Table 10.1: The Statistical Results of the Gamma Evaluation for the Prostate Patients

DTA [mm]	Dose difference [%]	MRI_u [%]	MRI_b [%]	P-value	Significant
2	2	62.3 (39.8-90.6)	74.0 (58.7-94.2)	$4.0 \cdot 10^{-4}$	S
2	3	73.9 (59.3-93.7)	79.3 (65.2-99.0)	$3.8 \cdot 10^{-3}$	S
3	3	79.9 (61.7-97.0)	84.1 (67.1-99.3)	$7.3 \cdot 10^{-3}$	S

Chapter 11

Discussion

The main focus in the investigation of the feasibility of MRI-only based RT, has been a statistical evaluation of DVH point for comparison of the dose calculations based on the CT and the density corrected MRIs.

A statistical analysis is sensitive to variation in the data. Clinical data always include variation. In our study the clinical variation can be caused by different tumour localisations in the same diagnostic group and differences in the patient geometry. Additionally, the treatment plan is based on a clinical evaluation of each patient, where individual restrictions have to be considered. Significant differences might not be detected due to a large variation in the diagnostic group. The size of the diagnostic group can also influence the ability to detect significant differences.

The DVH points are considered as highly clinically relevant. However, it should still be noted that the statistical analysis only describes similarities in the DVH points and not in the shape of the DVH. Moreover, the DVH does not contain spatial information regarding the dose distribution. This limitation in the DVH is not taken into further consideration in the statistical evaluation. Therefore some critical clinical differences between the CT and the density corrected MRIs might not be detected in the statistical analysis. The statistical analysis should therefore not be used as the only evaluation tool.

11.1 Head & Neck Patients

For the HN patients no significant differences were detected in the investigated DVH points for the target volumes and the OARs. However, in the visual inspection of the DVH shape for the PTV, it is clear that the MRI_u differs remarkable, although no significant difference was detected. The diagnostic group contains various differential diagnoses, the variation is therefore thought to be a result of the different tumour localisations. The MRI_b and the $MRI_{b,c}$ give results that are more similar to the CT for the target volumes than MRI_u. The positive effect of the bone and air cavity segmentation is expected due to a large presence of bone and air in the HN region. However, when comparing MRI_b with $MRI_{b,c}$, similar results are seen, indicating that the air segmentation does not contribute with results closer to the CT. Based on this detection, air segmentation is not found to be necessary for the density correction of MRI.

Investigating the OARs, it is seen that the standard deviations are notably higher than the target volumes. This is expected since the tumour is located differently in each patient, therefore the OARs are effected differently by the dose prescribed to the target volumes. Additionally, the treatment plan is optimized for the target volumes. However, the optimization is only performed to an extent where the first priority serial organs (medulla and brain stem) are not compromised [16]. This correspond well with our results where the first priority OARs have lower standard deviations, compared to the parotid glands which are third priority OARs.

Based on the DVH point investigation for medulla, both the $MRI_{b,c}$ and the MRI_b seems reasonable, since they provide a smaller maximum dose to medulla than the MRI_u and the CT. However, the shape of the DVHs for medulla indicates that the CT is more similar to the MRI_b than the $MRI_{b,c}$. Based on the shape of the DVHs and the percentage differences, the MRI_b is found to be the most suitable density correction for medulla.

From the statistical analysis, it is found that the MRI-based RT is a feasible alternative to the CT-based RT for the HN patients. Adding the visual inspection, it is found that the MRI_b gives the most feasible results, for both the OAR and the target volumes.

11.2 Sarcoma Patients

The statistical analysis of the sarcoma patients, shows that there are no significant difference when comparing the DVH points from the CT, the MRI_u and the MRI_b. These results are in correspondence with the subjective investigation of the DVH shapes. Therefore, it does not seem necessary to segment bone prior to density correction of the MRI.

For the investigated sarcoma patients the tumour is located in the extremities and the patients are treated with 3D CRT (two opposing fields). The field aperture is often shaped to avoid that the PTV coverage is affected by bone. Based on this, and the results of the investigation it seems reasonable to use the MRI_u, for the MRI-based RT of sarcoma patients.

11.3 Pelvic Patients

For the pelvic patients, no significant differences are found in the statistical analysis. The percentage differences for the MRI_u and the MRI_b with respect to the CT are within $\pm$ 1% for both the targets and the OARs. The MRI_b was thought to give results closer to the CT than the MRI_u, since the pelvic patients are treated with VMAT that gives continuously radiation in arcs and therefore also to some extent radiate bone. The unexpected result may be due to a large field size. The field is approximately 4 times larger than the field for the prostate patients (which showed significant difference for the investigated target volumes). However, it is more likely due to the small sample size. In Appendix D the effect of a small sample size in a statistical analysis is investigated for the prostate patients. It is found that an ANOVA of 5 prostate patients shows non significant results, even though significance is detected for the entire diagnostic group, containing 21 prostate patients. Therefore the consequence of a small diagnostic group, of 5 pelvic patients could influence the detection of differences between the dose distributions.

Evaluating the DVH for the OARs it is seen that they are very similar both in the overall shape and in the specific DVH points. Looking at the p-values for the organs at risk, they show highly non-significance, indicating very high similarity. The investigation of the OARs indicate, that bone segmentation is not necessary.
It was expected that MRI_b would be the appropriate choice for MRI-based RT. However this was not found in the investigation. Based on the evaluation MRI_b and MRI_u seems equally suitable.

11.4 Prostate Patients

11.4.1 Dose Volume Histogram Evaluation

Investigating the standard deviations for the target volumes and the OAR, the values are in general lower and more consistent compared to the other diagnostic groups. This is expected because of a large data set, and a small clinical variation caused by a similar tumour localisation in each patient.

For the OAR it was necessary to divide the prostate patients in groups dependent on the prescribed dose. However no significant difference was detected for any of the groups. It is not possible to see the differences in the DVHs for rectum for CT, MRI_u and MRI_b.

Evaluation of the target volumes shows that the investigated DVH points are significantly different. The following analysis using a paired t-test illustrates that the MRI_u differs significantly from both CT and MRI_b. These results indicate that a segmentation and density correction of bone is necessary prior to MRI-only based RT.

11.4.2 Gamma Volume Histogram Evaluation

A GVH investigation was performed for the PTV of the prostate patients, in order to complement the results found in the DVH investigation.

The performed gamma evaluation is slice based and the dose distributions are therefore only evaluated in the transaxial plane. A full 3D gamma evaluation will be more appropriate, since the acceptance criteria will also be evaluated in the z-direction. However, this feature was not available.

Prior to gamma evaluation, certain conditions have to be made, with regard to the data processing (described in Section 8.4). In the registration of the CT with the MRI, the rotation was not considered. The rotation information was excluded since the rotation is less than 1 degree in all directions for majority of the patients. However, the rotation will not have any impact in the z-direction since the evaluation is limited to the transaxial plane. In the transaxial plane the rotation could potentially influence the alignment of the coordinate system and therefore the results of the gamma investigation. Small errors in the alignment can contribute to a large error in the gamma investigation, since the pixel resolution in the transaxial plane is 2.5 mm for both the CT and the MRI and

the DTA is investigated for both 2 and 3 mm.

The gamma evaluation can only be used to compare the CT to the density corrected MRIs. There are no clinical guidelines used to evaluate the percentage of pixels within a region of interest that fulfil the gamma criteria. However, the evaluation can be used to compare the MRI_u and the MRI_b with the CT. In the paired t-test it is found that MRI_b is significantly better than the MRI_u. This is applicable for all investigated combinations of acceptance criteria.

The GVH evaluation supports the results found with the DVH investigation.

11.5 Delivery Techniques

The diagnostic groups are treated with different treatment techniques (see Section 8.1). The results for each diagnostic group are therefore related to the specific technique. The use of another technique may cause different results. The investigated data is real clinical data, and reflects the treatment procedures at the hospital. It has not been possible to evaluate the different techniques on the same diagnostic group, since the treatment plans were not available.

11.6 Patient Setup Verification

In Chapter 3, it is described how the current setup verification is based on DRRs created from CT information and radiographs taken with the LINAC. By eliminating the CT in RT the DRRs will not be available. Therefore, MRI-only requires new approaches for the patient setup. This has not been investigated in our study. However, Buhl et al. [10] showed that conduction of 3D MRI-CBCT was feasible for online patient setup verification in RT.
For prostate patients, another approach to patient verification without the CT could be a 2D matching of the gold seeds, which is visible both in the MRI (black due to signal loss) and the radiographs (white due to high density) acquired with the LINAC.
A third approach depends on a successful bone segmentation in MRI. This might be possible, with a the UTE sequence, as described in Section 4.2. If bone segmentation with MRI is possible the bone structures can be used for 2D matching with the radiographs. Prior to a clinical implementation of MRI-only based RT, patient setup verification using MRI needs to be investigated.

11.7 Previous Related Work

In the following, the results of the studies described in Chapter 2 are discussed and compared to our study.

Jonsson et al. compares the dose distributions based on a CT and a MRI. Our discussion of the results found by Jonsson et al. is focused on the investigation of the prostate- and the HN patients, as these groups are comparable to our study.

For the investigation of the prostate patients, Jonsson et al. chose a density correction of bone based on the electron density of the femoral bone (whole)- 1.33 g/cm^3. During a DVH inspection Jonsson et al. found that the DVH shows a clear under-dosage for the bulk density assigned CT. This indicates that the choice of electron density was not descriptive for the actual bone density. The electron density used by Jonsson et al. corresponds to an age of 30 years. However, the average age of the prostate patients are 67 years. In our study, the electron density is based on the average age of the prostate patients and an interpolation of age-dependent values from ICRU Report 46. This procedure was done in order to obtain the best representative bone electron density for the prostate patients.

Jonsson et al. finds that bulk density correction is necessary for prostate patients. The comparison of bulk density assigned MRI and CT is based on the difference in mean MU values of one DVH point. For the prostate patients the percentage deviation was found to be 0.2 %. These results are in accordance with the findings in our study. However, the results in our study shows a higher degree of similarity between CT and MRI_b, which is expected to be due to the choice of electron density for the femur bone.

A comparison between the CT and MRI based dose distributions was not performed for HN patients by Jonsson et al. due a to lack of MRI data. Therefore, the evaluation of HN patients is based a comparison of the CT and the bulk density assigned CT. Jonsson et al. finds that the chosen density value (cranium (whole) = 1.61 g/cm^3) for the HN patients provides a clinical acceptable agreement between the CT and the bulk density assigned CT, based on a DVH inspection [25]. As was displayed in Table 8.1 Section 8.2 the chosen bone electron density in our study is in accordance with the one used by Jonsson et al..

Another related study was performed by Lambert et al.[29], where a statistical analysis of absorbed dose values is used to compare the density corrected MRIs with a CT. An average electron density of bone for prostate patients is

determined to 1.19 g/cm^3, which corresponds to a HU equal to 288. The bone density is based on effective depth calculations. Lambert et al. do not provide the average age of the prostate patients. The electron density determined by Lambert et al. can therefore not be directly compared to the electron density used in our study.

Lambert et al. use one DVH point ($D_{98\%}$) to compare the dose for PTV in the density corrected MRIs with a CT gold standard. It is found that bulk density assigned MRI differs -1.3 % from CT and the unit density assigned MRI differs -2.6 % from CT [29]. These results show the same tendency as was found in our study, that MRI_b is closer to CT than MRI_u. In our study MRI_u is found to give a higher dose than CT. This difference is expected to be caused by different techniques, as Lambert et al. use 3D CRT. In a paired t-test, Lambert et al. finds that the CT is significantly different from the bulk density assigned MRI in $D_{98\%}$ for the 23 prostate patients with a prescribed dose of 70 Gy [29]. This observation differs from our study, where no significance was detected between the CT and the MRI_b for the PTV in the three investigated DVH points ($D_{98\%}$, $D_{2\%}$, D_{median}). Even though different results were found, we believe that our study is stronger since the statistical analysis is based on three DVH points.

For rectum, Lambert et al. investigate three volumes that receive a specific dose (V_{40Gy}, V_{60Gy}, V_{70Gy}). Lambert et al. finds that there is no significant difference between the density assigned MRIs and the CT [29]. In our study, other DVH points were investigated, with similar results.

The relevant studies mostly concern investigations for prostate patients. Therefore, it is not possible to compare previous studies with our results from the remaining diagnostic groups. Jonsson et al. includes HN patients in their study. However, due to limitations in the image acquisition, it was not possible for Jonsson et al. to obtain results of an comparison between the CT and the MRI. The fixation devices were not compatible with the head and neck coil in the MRI, which caused the lack of MRI data in the Jonsson et al. study. This limitation was not present in our study.

Both Jonsson et al. and Lambert et al. find that MRI-only based RT is achievable, and that bone segmentation and density correction is necessary for prostate patients. This is in accordance with the findings of our study, taken different delivery techniques in consideration.

Chapter 12

Conclusion

The investigated DVH points show that MRI-only based RT seems to be a feasible alternative to the CT-based RT. However, as previously discussed, the statistical analysis only describes similarities in the DVH points and not the shape of the DVH. For the HN patients, it was found the DVH points used for investigation of medulla did not reflect the shape of the DVH. For the remaining diagnostic groups, a larger resemblance were found between the DVH points and the overall shape of the average DVH.

For the HN patients, the statistical analysis of the DVH points showed that all density corrected MRIs were suitable. However, the visual inspection indicated that the MRI_b is more appropriate with results closer to the CT. Additionally, it was found that correction for air cavities had no significant effect.

For the pelvic and sarcoma patients, it was found that bone segmentation and density correction is not necessary in order to obtain results similar to the CT. However, the bone segmentation was expected to be necessary for the pelvic patients, since bone segmentation was found to be necessary for prostate patients. Pelvic and prostate patients are expected to give similar results, since they are treated with the same treatment technique in the same anatomical region. The lack of significance for the pelvic patients is thought to be caused by a small diagnostic group (5 patients).

For the prostate patients, the MRI_u differs significantly from MRI_b and CT, in both the DVH- and the GVH analysis. It is therefore concluded that a MRI_b is required for prostate patients.
Due to time restrains, the gamma evaluation of the remaining diagnostics groups were not included in our study. However, the GVH analysis is found suitable as a complement to the obtained DVH results for all the diagnostic groups.

The overall differences between CT and density corrected MRIs are acceptable. However, there might be unacceptable differences for the individual patients. The obtained results are consistent with those previous reported.

In general, MRI-only based RT is a suitable alternative to CT-based RT with specific density corrections required for each diagnostic group.

Appendix A

Abstract Accepted for ESTRO 31 Conference

Purpose

Multimodality imaging is increasingly combined for better tumour delineation. MRI provides additional soft-tissue contrast to CT, but registration of MRI and CT introduce a systematic error. Further, adaptive RT introduces an increase in scans and additional systematic errors. MRI-only based RT eliminates these errors and reduce the time and costs of a CT scan. The aim of this study is to investigate the dosimetric differences of a treatment plan when the dose calculation is based on MRI as compared to CT.

Methods

Four diagnostic groups are investigated; 12 Head and Neck (HN) patients treated with static IMRT, 6 sarcoma (extremities only) patients treated with APPA. 21 prostate and 5 pelvic (not prostate) patients treated with VMAT. Data for each patient contains a CT scan (Phillips Big Bore CT) and a T2 weighted MRI scan (1T Panorama Phillips) as well as a clinically approved treatment plan. The

treatment planning software is Eclipse v.10.0 (Varian Medical Systems). The dose calculation based on MRI data is evaluated in two different ways; a homogeneous density assigned MRI (MRI unit), where the entire body is assigned an HU equal to water and a heterogeneous density assigned MRI (MRI bulk) where in addition the CT segmented bone is transferred to the MRI and assigned an age dependent HU based on ICRU report 46. The CT based clinical treatment plan and structure set are registered to the corresponding MRI unit and MRI bulk. The body is outlined on both the MRI and the CT. The differences in dose distributions of the MRI bulk-, MRI unit- and CT data are quantified using DVH points. The reported DVH points for the PTV and CTV are Dmedian, D98% and D2% in accordance with ICRU report 83. The DVH points for the organs at risk are based on clinically guidelines used at our hospital and QUANTEC. One-way two-tailed ANOVA and paired t-test are used to investigate the differences in dose, based on MRI bulk, MRI unit and CT. The assumptions of ANOVA are found to be fulfilled, since data is normal distributed with constant variances.

Results

The results of differences in DVH points are displayed in the table. MRI-only based RT requires bulk density correction for prostate patients. For the remaining diagnostic groups both the unit- and bulk density corrected MRI show non-significant deviation for the selected DVH points. The mean differences are in the order of 2 %.

Conclusion

The investigated DVH points show that MRI-only based RT seems to be a feasible alternative to CT based RT. However, the analysis only describes similarities in DVH points and not in the shape of the DVH. Even though the mean differences are non-significant there might be unacceptable differences for the individual patient. In addition, significant differences may not be detected due to a large variance within a diagnostic group. The obtained results are consistent with those previous reported.

Diagnostic group	Volume (# of Patients)	Parameter	MRI unit [%] *	MRI bulk [%]*	Significant
Prostate	PTV(21)	D_{median}	1.3 ± 1.4	-0.0002 ± 1.1	A, B
		$D_{98\%}$	1.4 ± 1.9	-0.03 ± 1.7	A, B
		$D_{2\%}$	1.4 ± 1.3	-0.02 ± 1.0	A, B
	CTV(21)	D_{median}	1.3 ± 1.4	-0.005 ± 1.1	A, B
		$D_{98\%}$	1.4 ± 1.5	0.1 ± 1.3	A, B
		$D_{2\%}$	1.3 ± 1.4	0.1 ± 1.8	A, B
	Rectum**(12)	$D_{10\%}$	2.0 ± 1.7	0.6 ± 1.6	NS
		$D_{30\%}$	1.9 ± 2.5	0.8 ± 2.5	NS
		$D_{60\%}$	1.0 ± 3.0	0.2 ± 3.0	NS
	Rectum***(9)	$D_{10\%}$	2.2 ± 3.0	0.9 ± 3.0	NS
		$D_{30\%}$	0.8 ± 1.5	-0.008 ± 1.3	NS
		$D_{60\%}$	-0.006 ± 1.6	-0.7 ± 1.6	NS
Sarcoma	PTV(6)	D_{median}	-1.0 ± 1.8	-1.6 ± 3.0	NS
		$D_{98\%}$	-2.2 ± 19.1	-2.3 ± 19.2	NS
		$D_{2\%}$	-1.4 ± 3.2	-1.5 ± 3.6	NS
	CTV(6)	D_{median}	-1.2 ± 2.3	-1.5 ± 2.8	NS
		$D_{98\%}$	-0.9 ± 17.7	-1.1 ± 17.3	NS
		$D_{2\%}$	-1.6 ± 3.7	-1.6 ± 3.7	NS
Pelvic	PTV(5)	D_{median}	0.2 ± 1.5	-0.3 ± 1.6	NS
		$D_{98\%}$	-0.7 ± 2.3	-1.1 ± 2.0	NS
		$D_{2\%}$	0.6 ± 1.8	0.06 ± 2.1	NS
	CTV(5)	D_{median}	0.3 ± 1.5	-0.10 ± 1.7	NS
		$D_{98\%}$	-0.3 ± 2.2	-0.7 ± 1.9	NS
		$D_{2\%}$	0.6 ± 2.0	0.1 ± 2.2	NS
	Fem dxt.(5)	D_{mean}	-0.2 ± 3.8	0.09 ± 2.6	NS
		D_{max}	-0.2 ± 2.7	-0.70 ± 1.5	NS
	Fem sin.(5)	D_{mean}	0.2 ± 1.2	-0.3 ± 1.5	NS
		D_{max}	0.003 ± 1.8	-0.5 ± 1.5	NS
HN	PTV(12)	D_{median}	1.0 ± 2.3	-0.6 ± 1.3	NS
		$D_{98\%}$	1.0 4± 5.8	-0.5 ± 5.4	NS
		$D_{2\%}$	1.0 ± 2.3	-0.6 ± 1.1	NS
	CTV(12)	D_{median}	0.9 ± 2.3	-0.5 ± 1.7	NS
		$D_{98\%}$	-1.2 ± 4.2	-0.2 ± 3.7	NS
		$D_{2\%}$	1.1 ± 2.2	-0.5 ± 1.4	NS
	Medulla(12)	D_{max}	1,4 ± 11.6	-4.5 ± 12.8	NS
	Brainstem(9)	D_{max}	1.8 ± 12.6	-1.6 ± 11.8	NS
	Parotid sin(11)	D_{median}	-3.9 ± 18.0	-5.1 ± 19.0	NS
	Parotid dxt(12)	D_{median}	2.5 ± 29.3	1.0 ± 27.3	NS
	Larynx(7)	$D_{2/3\ Vol.}$	-2.0 ± 8.6	-2.5 ± 8.4	NS

* The percentage differences of MRI unit- and MRI bulk with respect to CT, in mean value ± two standard deviations. **For prostate patients with a prescribed dose of 70 Gy. ***For prostate patients with a prescribed dose of 78 Gy.
A: MRI unit vs. CT, B: MRI bulk vs. MRI unit, MRI bulk vs CT showed no significance. Significance level $p<0.05$. NS = Not significant. 80% of the the NS p-values are above 0.3.

Figure A.1

Appendix B

Poster Presented at the Department of Informatics and Mathematical Modelling December 2011

Herlev Hospital

Technical University of Denmark

MRI-only based Radiotherapy

An investigation of Prostate Patients

Marie Elgaard Korsholm & Line Winther Waring

Introduction

• In Denmark prostate cancer is the most frequent type of cancer for men [3]

• Every year 3,900 men are diagnosed with prostate cancer in Denmark [3]

All patients that are diagnosed with cancer and treated with radiotherapy will receive a computed tomography (CT) scan, which is used for dose planning, however most patients will also get an magnetic resonance imaging (MRI) scan. The image modalities have different advantages and are often combined to obtain all necessary information for optimal delineation of the tumour. Although multimodality imaging is used for delineation of the tumour, CT is currently the preferred choice for the treatment planning. However, the CT scan does not provide enough information for delineation of the tumour, with the accuracy required for sufficient treatment. The MRI scan is known to provide significant contrast of soft tissue, which is especially important when treating prostate cancer. The aim of this project is to investigate MRI-only based radiotherapy, as an alternative to CT-based radiotherapy.

A group of 21 prostate patients (the data set contains a CT scan, an MRI scan and a clinical treatment plan for all patients) were investigated for this purpose. This was done by comparing a dose plan based upon CT data, heterogeneous density corrected MRI (*MRI bulk*) and homogeneous density corrected MRI (*MRI unit*) respectively. Absorbed dose values recommended by International Commission on Radiation Units (ICRU)[1] and Herlev Hospital[2], are used to compare the results of the dose distributions of the CT scan, the unit density assigned MRI and the bulk density assigned MRI.

Background

Why MRI-only?

✓ Simplified workflow
✓ Reduce the cost of an extra scan
✓ Decrease the time consumption
✓ Great soft-tissue contrast for tumour delineation
✓ Eliminate the system registration error that occurs by combining the MRI scan and CT scan.

Fig 1. Registration of MRI and CT (Patient: Prost 19)

Method

In order to investigate the effect of replacing the CT scan with the MRI scan, the MRI data is evaluated in two different ways which is compared to the CT data .

MRI unit is a homogeneous density corrected MRI scan, where the body is assigned the Hounsfield Unit (HU) equal to water (HU=0). *MRI bulk* is heterogeneous density assigned data, where bone is segmented using the CT scan and afterwards transferred to the MRI scan. Bone is assigned HU = 349, based upon electron density information. The body is assigned the HU equal to water (HU=0).

A dose plan based upon the CT data is transferred to *MRI unit* and *MRI bulk* assigned data.

The dose distributions for CT data, *MRI bulk* density assigned data and *MRI unit* assigned data are then to be analyzed.

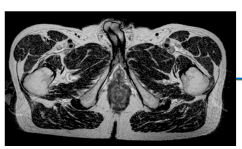

↑**Fig. 2:** An MRI scan for a patient with prostate cancer (Patient: Prost 11).

(a)

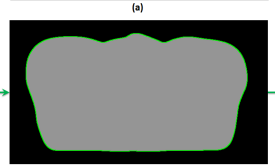

(b)

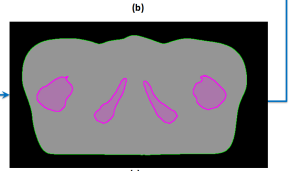

(c)

→ **Fig. 5:** The dose distributions calculated based upon **(a)** CT data **(b)** MRI unit density assigned data **(c)** MRI bulk density assigned data.
The dose distributions are shown relative to the prescribed dose. Red represents high dose, in contrast to blue that represents low dose. The areas with no color represented, receives less than 10 % of the prescribed dose (Patient: Prost 11).

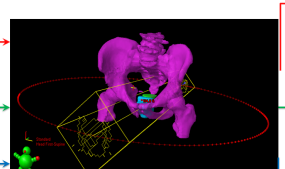

↑**Fig. 4:** A treatment plan that is based on a CT scan for a patient with prostate cancer (Patient: Prost 11).

←**Fig. 3: (a)** A CT scan for a patient with prostate cancer (Patient: Prost 11). **(b)** MRI unit assigned data (Patient: Prost 11). **(c)** MRI bulk assigned data (Patient: Prost 11).

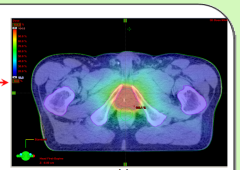

(a)

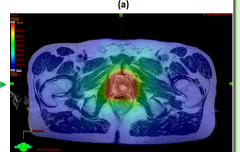

(b)

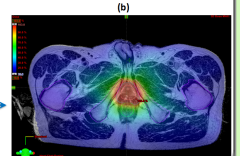

Dose Volume Histogram

A dose volume histogram (DVH) is a way to illustrate the cumulative 3D dose distribution, which makes it possible to analyze the 3D data in 2 dimensions.

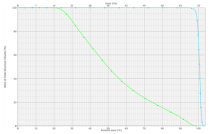

↑Fig. 6: The cummulative DVH shows the volume of a structure that receives a certain dose or higher

Absorbed dose values

Absorbed dose values recommended for **target volumes** by ICRU report 83[1]

For the planning target volume (PTV) and the clinical target volume (CTV):

- Dmedian : Absorbed dose received by 50 % of the volume
- D98%: The near minimum absorbed dose that covers 98 % of the volume
- D2%: The near maximum absorbed dose that covers 2 % of the volume

Absorbed dose values recommended for **Organs at Risk** by Herlev Hospital[2]

For rectum:

- D60% : 60 % of the volume receives less than 36 Gy.
- D30% : 30 % of the volume receives less than 54 Gy.
- D10% : 10 % of the volume receives less than 65 Gy.

↑Fig. 7: The target volumes investigated are the PTV and CTV. The organ at risk investigated is rectum (Patient: Prost11).

Results

The results of the investigation between MRI bulk assigned data, MRI unit assigned data and CT are shown below.

Volume	Parameter	Method	Method	P-value
PTV	D_{median}	CT	MRI unit	$6.8 \cdot 10^{-7}$
		MRI bulk	MRI unit	$6.1 \cdot 10^{-6}$
		CT	MRI bulk	0.97
	$D_{98\%}$	CT	MRI unit	$1.4 \cdot 10^{-3}$
		MRI bulk	MRI unit	$3.1 \cdot 10^{-3}$
		CT	MRI bulk	0.88
	$D_{2\%}$	CT	MRI unit	$2.4 \cdot 10^{-7}$
		MRI bulk	MRI unit	$5.2 \cdot 10^{-7}$
		CT	MRI bulk	0.88
CTV	D_{median}	CT	MRI unit	$1.2 \cdot 10^{-6}$
		MRI bulk	MRI unit	$6.9 \cdot 10^{-6}$
		CT	MRI bulk	0.77
	$D_{98\%}$	CT	MRI unit	$4.9 \cdot 10^{-6}$
		MRI bulk	MRI unit	$7.3 \cdot 10^{-5}$
		CT	MRI bulk	0.27
	$D_{2\%}$	CT	MRI unit	$5.2 \cdot 10^{-7}$
		MRI bulk	MRI unit	$9.1 \cdot 10^{-6}$
		CT	MRI bulk	0.47

↑ Table 1: A paired Wilcoxon rank sum test for comparison of CT data, MRI bulk density assigned data and MRI unit density assigned data (21 prostate patients).

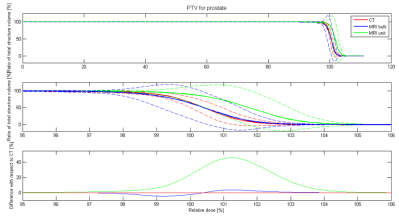

↑Fig. 8 : PTV (21 prostate patients). The top figure shows the average DVHs of the prostate patients. The middle figure is a cut away from the top figure. The bottom figure shows the differences in DVHs with CT as reference. The dotted lines are ±two standard deviations.

Prescribed dose	Volume	Parameter	Method	Method	P-value
70Gy	Rectum	$D_{10\%}$	CT	MRI unit	$4.9 \cdot 10^{-4}$
			MRI unit	MRI bulk	$4.9 \cdot 10^{-4}$
			CT	MRI bulk	0.42
		$D_{30\%}$	CT	MRI unit	$3.4 \cdot 10^{-3}$
			MRI unit	MRI bulk	$4.9 \cdot 10^{-4}$
			CT	MRI bulk	0.42
		$D_{60\%}$	CT	MRI unit	$6.4 \cdot 10^{-2}$
			MRI unit	MRI bulk	$4.9 \cdot 10^{-4}$
			CT	MRI bulk	0.57

↑ Table 2: Paired Wilcoxon rank sum test for comparison of CT data, MRI bulk density assigned data and MRI unit density assigned data for rectum, 70 Gy (12 prostate patients).

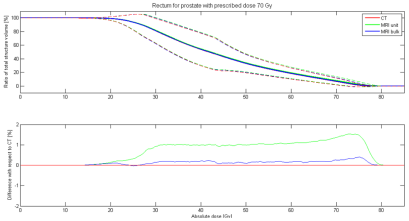

↑Fig. 9: Rectum, 70 Gy (12 prostate patients).The top figure shows the average DVHs of the prostate patients. The bottom figure shows the differences in DVHs with CT data as reference. The dotted lines are ±two standard deviations.

Conclusion

It was found that there is no significant difference between MRI bulk assigned data and CT data for the planning target volume, clinical target volume and rectum. However, there was found significant difference between MRI unit assigned data and CT data for the planning target volume, clinical target volume and rectum. This is also the case for the test between MRI unit assigned data and MRI bulk assigned data.

The MRI bulk density assigned data gives results that are closer to the CT data than MRI unit density assigned data. Moreover, MRI unit assigned data gives in general higher values than MRI bulk assigned data and CT data.

Based on these results it can be concluded that it is reasonable to use MRI bulk assigned data in MRI-only radiotherapy.

Supervisors: Jens Edmund, Ph.D. (Herlev Hospital), Associate Professor Rasmus Paulsen, Ph.D., Department for Mathematical Modelling (DTU), Claus F. Behrens, Ph.D. (Herlev Hospital)

References: [1] HO Wycko. ICRU report 83 prescribing, recording, and reporting photon-beam intensity-modulated radiation therapy (IMRT). Journal of the ICRU, 48(2):20112011. [2] L. Sengeløv. Retningslinjer for patienter med prostatacancer. 2010. [3] Kræftens bekæmpelse. Nøgletal. 2009

Appendix C

Two-way ANOVA for Evaluation of Rectum

In the investigation of the prostate patients, the statistical analysis of the DVH points for rectum is performed separately for the patients with a prescribed dose of 78 Gy and 70 Gy, respectively. When evaluating the DVH in Figure 9.6 in Section 9.1.4 it is seen that the DVHs are similar in shape. However, the DVHs are visually easily separated. Therefore, it is of interest to investigate if the differences are due to the different prescription dose or random variation in the patient data.

The data is found to be normally distributed with constant variances. Therefore, the investigation is based on a two-way ANOVA. The two investigated factors are; the prescribed dose (two levels: 78 Gy and 70 Gy) and the modality (three levels: CT, MRI_u and MRI_b). The investigation is performed without taking an interaction term into consideration, since there are no replicates. It is tested if the the mean value of the observations grouped by one factor is the same as the mean value of the observations grouped by the other factor [24, p. 450-454].

The results of the two-way ANOVA are displayed in Table C.1 for each investigated DVH point. It is seen that the prescribed dose factor is significant for all three investigations ($D_{10\%}$, $D_{30\%}$, $D_{60\%}$). This indicates that the prescribed dose cannot be neglected. This is confirmed with a model reduction were it is found that the prescribed dose factor cannot be excluded from the analysis.

Table C.1: Two-way ANOVA table for Rectum

Volume	DVH point	Factor	P-value
Rectum	$D_{10\%}$	Modality	0.36
		Prescribed dose	$3.5 \cdot 10^{-8}$
Rectum	$D_{30\%}$	Modality	0.92
		Prescribed dose	$7.2 \cdot 10^{-5}$
Rectum	$D_{60\%}$	Modality	0.98
		Prescribed dose	$6.0 \cdot 10^{-3}$

These findings indicate that the prescribed dose must be taken into account when evaluating the effect of density correction.

Appendix D

Evaluation of the Effect of Sample Size

An ANOVA is used to detect if there are significant differences when comparing the density assigned MRIs with the CT. It is found that no significant differences could be detected for the pelvic patients, while the prostate patients differed significantly for the target volumes. The two diagnostic groups were expected to give similar results, due to the same treatment region and delivery technique. The different statistical results are suspected to be due to the small sample size for the pelvic patients.
In order to investigate this an ANOVA is performed based on 5 randomly selected prostate patients. This procedure was repeated 10 times for each DVH point for the PTV and the CTV. The results of the investigation are summarised in Figure D.1. When evaluating the target volumes for the 5 randomly selected prostate patients, they will occasionally show non significant difference, even though the entire prostate group differs significantly. This indicates that a small sample size influence the reliability of the statistical analysis.

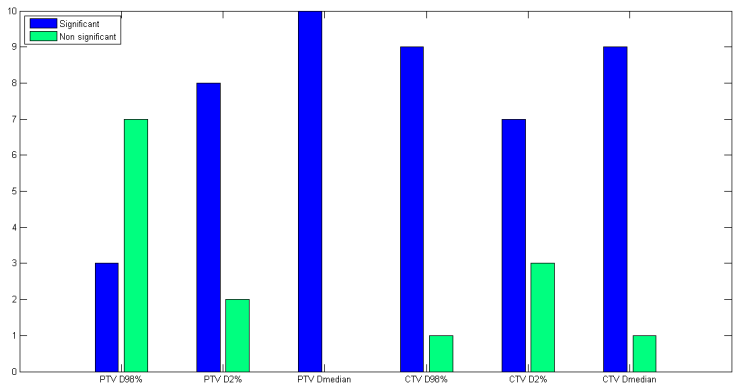

Figure D.1: The statistical results based on an ANOVA performed with 5 randomly selected prostate patients and 10 repetitions

Bibliography

[1] http://http://www.cerr.info.

[2] http://www.varian.com/us/oncology/treatments.

[3] http://varian.mediaroom.com/index.php?s=13&cat=22&mode=gallery.

[4] http://www.prostate-cancer-radiotherapy.org.uk/standard_ebrt.htm.

[5] Samlet oversigt over bækken constrains, Herlev: Onkologisk afdeling.

[6] Prescribing, recording, and reporting photon-beam IMRT. *International Commission on Radiation Units and Measurements. ICRU Report 83*, 2010.

[7] G.C. Barnett, C.M.L. West, A.M. Dunning, R.M. Elliott, C.E. Coles, P.D.P. Pharoah, and N.G. Burnet. Normal tissue reactions to radiotherapy: towards tailoring treatment dose by genotype. *Nature Reviews Cancer*, 9(2):134–142, 2009.

[8] M.C. Biagiolo and S.E. Hoffe. Emerging technologies in prostate cancer radiation therapy: improving the therapeutic window. *Cancer Control*, 17:223–232, 2010.

[9] T. Bortfeld. IMRT: a review and preview. *Physics in medicine and biology*, 51:R363, 2006.

[10] S.K. Buhl, A.K. Duun-Christensen, B.H. Kristensen, and C.F. Behrens. Clinical evaluation of 3D/3D MRI-CBCT automatching on brain tumors for online patient setup verification-a step towards MRI-based treatment planning. *Acta Oncologica*, 49(7):1085–1091, 2010.

[11] J.T. Bushberg. *The essential physics of medical imaging.* Williams & Wilkins, 2002.

[12] J. Dobbs and A. Barrett. *Practical radiotherapy planning.* Edward Arnold Pubs. Ltd., Baltimore, MD, 1985.

[13] RE Drzymala, R. Mohan, L. Brewster, J. Chu, M. Goitein, W. Harms, and M. Urie. Dose-volume histograms. *International Journal of Radiation Oncology* Biology* Physics*, 21(1):71–78, 1991.

[14] J. Eric. Hall. radiobiology for the radiologist. 2000.

[15] M.D.C. EVANS et al. Computerized treatment planning systems for external photon beam radiotherapy. *Review of Radiation Oncology Physics: A Handbook for Teachers and Students.*

[16] Odense Universitetshospital Aalborg Sygehus Aarhus Universitetshospital FinsenCenteret, KAS Herlev. *DAHANCA 2004 - Retningslinjer for strålebehandling af hoved-hals cancer(cavum oris, pharynx, larynx), inklusiv IMRT vejledning*, volume 3. 2004.

[17] L. Hanna, T. Crosby, F. Macbeth, and MyiLibrary. *Practical clinical oncology.* Cambridge University Press, 2008.

[18] J.P. Hornak. The basics of MRI.

[19] P.J. Hoskin and V. Goh. *Radiotherapy in practice: imaging*, volume 4. Oxford Univ Pr, 2010.

[20] S. Huq, P. Mayles, P.B. de Carcer, et al. Transition from 2-d radiotherapy to 3-d conformal and intensity modulated radiotherapy. Technical report, IAEA-TECDOC-1588, International Atomic Energy Agency, 2008.

[21] M. Jensen and J. E. Wilhjelm. *CT scanning.* 2007.

[22] P.H. Jensen, B. Lauridsen, J. Søgaard-Hansen, and L. Warming. *Kursus i helsefysik.* Forskningscenter Risø, 2001.

[23] A. Johansson, M. Karlsson, and T. Nyholm. CT substitute derived from MRI sequences with ultrashort echo time. *Medical Physics*, 38:2708, 2011.

[24] R.A. Johnson. *Probability and statistics for engineers*, volume 13. 2005.

[25] J.H. Jonsson, M.G. Karlsson, M. Karlsson, and T. Nyholm. Treatment planning using MRI data: an analysis of the dose calculation accuracy for different treatment regions. *Radiation Oncology*, 5(1):62, 2010.

[26] V. Keereman, Y. Fierens, T. Broux, Y. De Deene, M. Lonneux, and S. Vandenberghe. MRI-based attenuation correction for PET/MRI using ultrashort echo time sequences. *Journal of Nuclear Medicine*, 51(5):812, 2010.

[27] F.M. Khan and S. Stathakis. *The physics of radiation therapy*, volume 37. 2010.

[28] M.E Korsholm, L.W Waring, R.R Paulsen, and J.E Edmund. Statistical analysis of MRI-only based dose planning. *ESTRO abstract*, 2012.

[29] J. Lambert, P.B. Greer, F. Menk, J. Patterson, J. Parker, K. Dahl, S. Gupta, A. Capp, C. Wratten, C. Tang, et al. MRI-guided prostate radiation therapy planning: Investigation of dosimetric accuracy of MRI-based dose planning. *Radiotherapy and Oncology*, 98(3):330–334, 2011.

[30] R Larsen. 02505 course note, medical image analysis. 2008.

[31] D.A. Low, W.B. Harms, S. Mutic, and J.A. Purdy. A technique for the quantitative evaluation of dose distributions. *Medical Physics*, 25:656, 1998.

[32] L.B. Marks, E. D. Yorke, Jackson A., R. K. Ten Haken, L. S. Constine, A. Eisbruch, S. M. Bentzen, J. Nam, and J. O. Deasy. Use of normal tissue complication probability models in the clinic. *International Journal of Radiation Oncology* Biology* Physics*, 76(3):S10–S19, 2010.

[33] P. Mayles, A.E. Nahum, and J.C. Rosenwald. *Handbook of radiotherapy physics: theory and practice*. Taylor & Francis, 2007.

[34] D.W. McRobbie, E.A. Moore, and M.J. Graves. *MRI from picture to proton*. Cambridge Univ Pr, 2007.

[35] Crawley M.J. *Statistics: an introduction using R*. Wiley, 2005.

[36] Crawley M.J. *The R book*. Wiley, 2007.

[37] S. Morris. *Radiotherapy physics and equiptment*. 2001.

[38] International Commission on Radiation Units and Measurements. ICRU Report 46. Photon, electron, proton and neutron interaction data for body tissues. 1992.

[39] A. Oppelt. *Imaging systems for medical diagnostics: fundamentals, technical solutions, and applications for systems applying ionizing radiation, nuclear magnetic resonance, and ultrasound*. Wiley-VCH, 2005.

[40] K. Otto. Volumetric modulated arc therapy: IMRT in a single gantry arc. *Medical physics*, 35:310, 2008.

[41] CC Parker, A. Damyanovich, T. Haycocks, M. Haider, A. Bayley, and CN Catton. Magnetic resonance imaging in the radiation treatment planning of localized prostate cancer using intra-prostatic fiducial markers for computed tomography co-registration. *Radiotherapy and oncology*, 66(2):217–224, 2003.

[42] E.B. Podgorsak and Agency International Atomic Energy. *Radiation oncology physics*. International Atomic Energy Agency, 2005.

[43] J.A. Purdy, J.M. Michalski, J. Bradley, S. Vijayakumar, C.A. Perez, and S.H. Levitt. Three-dimensional treatment planning and conformal therapy. *Technical Basis of Radiation Therapy*, pages 179–202, 2006.

[44] W. Schlegel. If you can't see it, you can miss it: the role of biomedical imaging in radiation oncology. *Radiation protection dosimetry*, 139(1-3):321, 2010.

[45] L. Sengeløv. Retningslinjer for patienter med prostatacancer. 2010.

[46] A. L. Spanggaard and C. Hangaard. Strålebehandling. *Herlev Hospital, Onkologisk afdeling*, 2007.

[47] E. Spezi and D.G. Lewis. Gamma histograms for radiotherapy plan evaluation. *Radiotherapy and oncology*, 79(2):224–230, 2006.

[48] E. Spezi, DG Lewis, and CW Smith. A dicom-rt-based toolbox for the evaluation and verification of radiotherapy plans. *Physics in medicine and biology*, 47:4223, 2002.

[49] H.C. Thode. *Testing for normality*, volume 164. CRC, 2002.

[50] A. Van Esch, D.P. Huyskens, C.F. Behrens, E. Samsøe, M. Sjölin, U. Bjelkengren, D. Sjöström, C. Clermont, L. Hambach, and F. Sergent. Implementing rapidarc into clinical routine: A comprehensive program from machine qa to tps validation and patient qa. *Medical Physics*, 38:5146, 2011.

[51] L.W Waring and M.E Korsholm. MRI-only based radiotherapy. *Poster presented at the Department of informatics and mathematical modelling*, 2011.

[52] S. Webb and D. McQuaid. Some considerations concerning volume-modulated arc therapy: a stepping stone towards a general theory. *Physics in Medicine and Biology*, 54:4345, 2009.

[53] B. Zitova and J. Flusser. Image registration methods: a survey. *Image and vision computing*, 21(11):977–1000, 2003.